DESIGN AND VALIDATION OF A VERSATILE THERMOMECHANICAL FATIGUE TEST SYSTEM RETROFIT KIT

By

HADEN RUSSELL GLASGOW

Bachelor of Science in Aerospace Engineering
Oklahoma State University
Stillwater, Oklahoma
2021

Bachelor of Science in Mechanical Engineering
Oklahoma State University
Stillwater, Oklahoma
2021

Submitted to the Faculty of the
Graduate College of the
Oklahoma State University
in partial fulfillment of
the requirements for
the Degree of
MASTER OF SCIENCE
May, 2023

DESIGN AND VALIDATION OF A VERSATILE THERMOMECHANICAL FATIGUE TEST SYSTEM RETROFIT KIT

Thesis Approved:

Dr. Kurt Rouser

Thesis Advisor

Dr. Hadi Noori

Dr. Sandip Harimkar

ACKNOWLEDGMENTS

I would like to thank my advisor Dr. Kurt Rouser for his guidance and instruction over the course of my graduate career. I would also like to thank my committee members Dr. Hadi Noori and Dr. Sandip Harimkar for their insight and assistance during my graduate career. Thank you to my family for your unconditional love and support, and for motivating me to reach my goals. Thank you to Bryan Pizana for your knowledge and assistance over the course of this study. Thank you to my friends for your encouragement and support throughout my undergraduate and graduate studies here at Oklahoma State University.

Acknowledgments reflect the views of the author and are not endorsed by committee members or Oklahoma State University.

Name: HADEN RUSSELL GLASGOW

Date of Degree: MAY, 2023

Title of Study: DESIGN AND VALIDATION OF A VERSATILE THERMOMECHANICAL FATIGUE TEST SYSTEM RETROFIT KIT

Major Field: MECHANICAL AND AEROSPACE ENGINEERING

Abstract: This paper presents the design and experimental validation of a low-cost thermomechanical fatigue (TMF) test system that can be retrofitted to a dynamic load universal test machine with minimal modifications. The motivation for this study is to fabricate a cost-effective and universally compatible thermomechanical fatigue testing system that has the ability to evaluate ferromagnetic aerospace materials. Typically, TMF test systems are available from an original equipment manufacturer (OEM) for a complete system or as a retrofit kit, costing as much as $500,000 or $300,000 , respectively. Also, OEM equipment is not interchangeable with other systems and requires manufacturer specific components to operate. An analytical study was performed to design and size components to meet American Society for Testing and Materials test standard E2368 with minimal cost. The resulting design consists of an Arduino micro controller that reads instrumentation signals and a package of components that do not rely on interfacing with external software or hardware to perform a thermomechanical fatigue test. The specific test system hardware components consist of a 10 kW induction heater, industrial chiller for induction coil operation, cooling flow nozzles coupled with an air compressor, thermocouples mounted outside the gauge section, an infrared pyrometer for temperature monitoring within the specimen gauge section, and an axial extensometer to synchronize the thermal and mechanical loading cycles. Validation of the system is completed by evaluating the synchronization of thermal and mechanical loading cycles over a test matrix with varying cycle times and loading parameters. The system operation follows a set mechanical load and alters the thermal profile in response to match the profiles. Initial experiments were conducted to tune heating and cooling process parameters to achieve minimal load variance between mechanical and thermal loading profiles. Subsequent experiments characterized response time variance at different loading cycle frequencies and amplitudes. From experimental testing, it was determined the system control scheme is correctly designed with existing components to maintain synchronization within a certain frequency band and amplitude band for an indefinite number of cycles. This study enables development of fatigue model validation for predicting needed preventative maintenance, and improving supply chain management. Further recommendations for this system may include an improved induction heater that uses digital active control to regulate power output magnitude and an improved air cooling system to regulate air flow rate in real time.

TABLE OF CONTENTS

LIST OF TABLES

LIST OF FIGURES

CHAPTER I

INTRODUCTION

1.1 Motivation

Materials used in jet engines, specifically turbine and compressor stages, operate in demanding environments. Temperatures in the turbine stage can reach over 3000°F in some engines and blades can be subjected to thousands of RPM that result in thousands of pounds of centripetal loading on the super-heated materials. The parts and materials utilized in these extreme operating conditions must be carefully selected and tested to ensure both safety and operability. To predict the failure modes and estimate part life-cycles, the materials must be evaluated with the assistance of a thermomechanical fatigue testing apparatus. The development of a versatile thermomechanical fatigue test capability is driven by the need for more accessible and affordable methods to assess the fatigue properties of various conventional and additive manufactured materials in the aerospace industry. Commercially available fatigue test machines are often expensive complex, and require specialized facilities and employees to operate, making it difficult for small-scale organizations to conduct such testing. Therefore, there is a critical need for a low-cost alternative that gives a TMF system with open architecture to accommodate a large variance in emerging additively manufactured materials. With testing of stochastic nature, such as any fatigue testing, there is great value in enabling more researchers to provide a higher volume of reliable data. This capability can provide valuable insight into the performance of materials and components by identifying failure modes to improve the

design and manufacturing process. This information is crucial to the development of safer and more reliable parts to meet the demanding requirements of the aerospace industry, among others.

1.2 Proposed Solution

The proposed solution approach for the development of a versatile thermomechanical fatigue testing capability aims to provide a cost-effective solution that meets the system performance requirements. The basic design consists of a material heater, material cooler, temperature instrumentation, strain instrumentation, and a control system, which all interface onto a single retrofitted kit that is then universally compatible with any existing static or dynamic test machine. The approach involves a thorough analysis and design of the system components individually, with a focus on optimizing performance while maintaining cost-effectiveness. From this analysis the system progresses through multiple design iterations to improve the performance, reliability, and accuracy of each component. This approach also takes into consideration the design characteristics of similar existing test systems, such as the MTS retrofitted system displayed in Figure 1.1, as guidance for solutions to common design challenges when attempting to operate at the extreme desired conditions.

The design process considers factors such as temperature monitoring accuracy, reduction of thermal gradients within the specimen, thermal and mechanical loading precision, and environmental stability, among others. To achieve a balance between performance and cost, commercially available components are incorporated wherever possible and low-cost, custom-made components are utilized only where necessary. The proposed solution also includes a robust control and data acquisition system that ensures accurate and reliable data collection during testing. The control system will allow for automated testing, including an active control loop for the synchronization of thermal and mechanical loading cycles. The thermal loading is actively modified

Figure I.1: MTS Thermomechanical Fatigue Test System

to match an independent mechanical loading profile. TMF testing can be performed under stress controlled or strain controlled conditions depending upon the intended control method, and utilizing a strain controlled method can be more beneficial as it results in a more versatile system. Test specimen material characteristics dictate the operating ranges of testing, and specimens are limited to only ferromagnetic materials due to the inductive nature of heating.

1.3 Research Objectives

A goal of this study is to design a versatile thermomechanical fatigue test system and validate system operability to assist in the study of advanced metals commonly used in aircraft and aircraft engines. TMF testing capabilities are intended to support the future work of creating analytical models in the advancement of digital twin software to increase the reliability and improve preventative maintenance for parts. Prior to this study, the most advanced testing capability available to propulsion researchers in some areas were high-cycle and low-cycle fatigue testing performed on

dynamic loading machines. Parts and materials which are designed to be subjected to both extreme temperature and mechanical loading simultaneously require a form of experimental evaluation readily accessible to validate and assist modeling efforts. This design strives to achieve a universally compatible and straightforward testing apparatus with experimental validation of the system testing limits and operability.

As such, the research objectives are as follows:

1. Design a versatile thermomechanical fatigue test system retrofit kit that meets the operating requirements set forth by the relevant ASTM E2368 testing standards to test Inconel 718

2. Analytically evaluate the system performance and ability to synchronize the thermal and mechanical loading profiles

3. Experimentally validate the ability of the system to synchronize thermal and mechanical loading profiles

CHAPTER II

Background and Theory

2.1 Common Aerospace Ferromagnetic Materials

Aerospace ferromagnetic materials refer to materials that are used in the construction of aerospace equipment such as gas turbine engines, aircraft structures, and space vehicles. These materials are chosen based on their specific properties, including strength, corrosion resistance, thermal stability, and their ability to withstand high-temperature environments.

Common aerospace ferromagnetic materials include:

1. Nickel-based alloys: These materials are used in gas turbine engines- specifically in turbine stages- due to their high strength, excellent corrosion resistance, and good thermal stability at high temperatures. Some of the most common nickel-based alloys include Inconel, Hastelloy, and Waspaloy.

2. Titanium alloys: Titanium alloys are used in aircraft structures and compressor stages due to their high strength-to-weight ratio and excellent corrosion resistance. Some of the most common titanium alloys include Ti-6Al-4V and Ti-6Al-2Sn-4Zr-2Mo.

3. Stainless steels: Stainless steels are used in gas turbine engines for stationary components such as casings that undergo high-temperature and low-mechanical loads due to their excellent corrosion resistance and good mechanical properties.

Some of the most common stainless steels used in aerospace include 304, 316, and 321 stainless steel.

One of the major problems in gas turbine engines is thermomechanical fatigue (TMF), which can lead to crack propagation and ultimately failure of the component. TMF occurs due to the combination of cyclic mechanical loading and high-temperature exposure, which causes the material to experience significant deformation, creep, and crack propagation. Creep refers to the gradual deformation of a material under a constant load, while crack propagation is the growth of a crack in a material under cyclic loading. Both of these processes can significantly reduce the lifespan of a gas turbine engine and increase maintenance costs. To address this issue, the aerospace industry is turning to the use of digital twins. Digital twins are virtual replicas of physical systems that use real-time data to simulate the behavior of the system and predict potential problems. By using digital twins, manufacturers can monitor the health of gas turbine engines in real-time and predict potential failures before they occur. This allows for preventive maintenance to be carried out, reducing downtime and improving the efficiency of supply chain management.

2.2 Thermomechanical Fatigue Testing Fundamentals

Thermomechanical fatigue refers to a testing mechanism where uniform, cyclic thermal and mechanical loading are applied simultaneously to the gauge section of a certain test specimen. The two loading parameters are typically applied in either an "in-phase" or "out-of-phase" configuration. "In-phase" cyclic loading refers to a condition where the thermal and mechanical maximum and minimum loads occur at the same time steps. Alternatively, "Out-of-phase" cyclic loading refers to a condition where the thermal loading waveform is shifted half of a cycle period so that the maximum mechanical loading occurs at the minimum temperature, and vice-versa. [2] Both of the loading types are illustrated further in Fig.1.

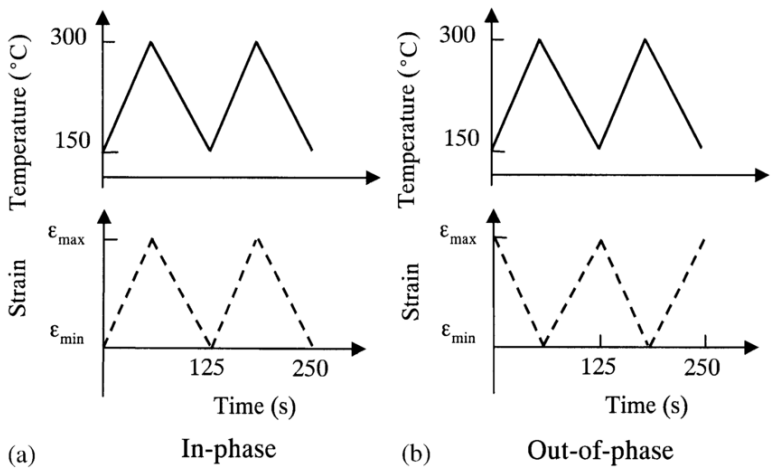

Figure II.1: TMF Loading Waveforms [15]

To achieve an intended mechanical strain range for the test, strain from the thermal loading must be assessed and compensated for. To compensate for the thermal strain during a test, a specimen is cycled through the intended temperature range while subjected to zero mechanical load with an axial extensometer measuring the resulting strain from thermal expansion of the material. The extensometer output is recorded and then implemented into the control program such that the recorded strain at each temperature is subtracted from the time-relative applied mechanical strain to obtain the intended overall strain value for every point in the cycle range. The previously discussed method is the more complex testing method, as TMF testing can also be performed under a load control mode where the strain does not need to be assessed and accounted for.

When selecting hardware for a TMF system, there are several important factors to consider. These include the type of testing machine, the temperature and strain control system, the specimen holder, the extensometer, and the heating and cooling system. The type of testing machine is crucial for TMF testing. Closed-loop electrohydraulic, servo-controlled, axially loaded machines are typically used for TMF testing because they allow for precise control over temperature and strain. These machines provide the necessary force to apply the mechanical stress and have the ability

to adjust the stress level based on the thermal strain compensation. The temperature and strain control system is also critical for TMF testing. The system should be capable of providing accurate and consistent temperature and strain waveforms. The temperature control system should be able to heat and cool the specimen quickly and efficiently, with a minimal temperature gradient. The strain control system should be able to maintain a constant strain range throughout the test. The specimen holder (or grip) is another important component of a TMF system and should be designed to minimize the risk of buckling in compression, provide a uniform strain distribution over its whole gauge portion, and allow the extensometer to measure the strain without interference or slippage. The holder should also be able to accommodate different types of specimens and have the ability to adjust to various specimen geometries. The extensometer is a critical component for measuring the mechanical strain during the TMF test. It should have high accuracy, precision, and resolution, with a low noise level. The extensometer should also be able to withstand high temperatures and be resistant to electromagnetic interference. Finally, the heating and cooling system is an essential component of a TMF system. The system should be able to heat and cool the specimen quickly and uniformly, without inducing thermal gradients. The system should also be able to maintain the desired temperature range throughout the test.

2.3 Relevant Working Engineering Principles

The following subsections outline the major working engineering principles applied in the system design processes.

2.3.1 Inductive Heating

Induction heating in a TMF system involves the generation of an alternating magnetic field by the induction coil, which induces electrical currents within the specimen,

causing it to heat up due to its resistance to the current. The magnitude of the induced current and therefore the amount of heating can be controlled by the following equations:

$$I = \frac{V}{R} \tag{2.3.1}$$

$$P = IV \tag{2.3.2}$$

where I is the current induced in the specimen, V is the voltage supplied to the induction coil, R is the resistance of the specimen, and P is the power supplied to the specimen.

The power supplied to the specimen can also be controlled by adjusting the frequency of the electrical energy supplied to the induction coil. The relationship between the frequency and the skin depth of the material is given by:

$$\delta = \sqrt{\frac{2}{\omega\mu\sigma}} \tag{2.3.3}$$

where δ is the skin depth, ω is the angular frequency, μ is the magnetic permeability of the material, and σ is the electrical conductivity of the material. The skin depth is an important variable to consider when sizing specimens and determining the operating frequency of the induction coil as a non-ideal selection of this parameter can lead to an axial temperature gradient within the specimen due to skin heating effects. Skin heating effects refer to the fact that the induced current density decreases exponentially with depth from the surface of the specimen. This means that the outer layer of the specimen will heat up more quickly than the inner layers. The skin depth equation, mentioned earlier, can be used to calculate the depth at which the current density has decreased to 1/e (approximately 37%) of its value at the surface.

Eddy current heating is caused by the circulation of electrical currents within the specimen due to the changing magnetic field produced by the induction coil. These

currents generate their own magnetic field, which opposes the original magnetic field and causes a loss of energy in the form of heat. This effect can be controlled by adjusting the frequency of the electrical energy supplied to the induction coil, as mentioned earlier.

Hysteresis heating occurs due to the magnetic properties of the specimen. When a magnetic material is subjected to a changing magnetic field, it undergoes hysteresis, which leads to the dissipation of energy in the form of heat. This effect is also controlled by adjusting the frequency of the electrical energy supplied to the induction coil.

With an induction heater that has variable control parameters, the controller can be programmed to follow a specific temperature profile using proportional-integral-derivative (PID) control algorithms. The temperature controller adjusts the power supplied to the specimen using the following equation:

$$P = K_p e + K_i \int e dt + K_d \frac{de}{dt} \tag{2.3.4}$$

where P is the power supplied to the specimen, e is the error between the desired temperature and the measured temperature, and Kp, Ki, and Kd are the proportional, integral, and derivative gains of the controller, respectively.

2.3.2 Emissivity

Emissivity is the ability of a material to emit or absorb electromagnetic radiation, particularly in the infrared region of the electromagnetic spectrum. In a TMF system, emissivity plays an important role in the accurate measurement of specimen temperature using an infrared pyrometer. The amount of infrared radiation emitted by a material is proportional to its emissivity, which can vary with temperature. The emissivity of a material can be described by the following equation:

$$\varepsilon = \frac{E}{\sigma T^4} \tag{2.3.5}$$

where ϵ is the emissivity of the material, E is the total energy radiated by the material, σ is the Stefan-Boltzmann constant, and T is the temperature of the material.

As the temperature of the material changes, its emissivity can also change. This can lead to errors in temperature measurement using an infrared pyrometer if the emissivity is not taken into account. To compensate for changes in emissivity, pre-test preparations must include placing the specimen in a furnace chamber with the infrared pyrometer measuring the temperature of the specimen against the known furnace temperature across the intended temperature testing range. This allows a relationship to be obtained for the actual temperature of the specimen versus the measured temperature, and this relationship can then be incorporated into the post-processing procedures of the control system.

2.3.3 Heat Transfer

Heat transfer is a fundamental aspect of thermomechanical fatigue testing, and there are three main modes of heat transfer: conduction, convection, and radiation.

Conduction is the transfer of heat through a solid material due to a temperature gradient. The rate of heat transfer through conduction is governed by Fourier's law:

$$\dot{Q}_{\text{cond}} = -kA\frac{dT}{dx} \tag{2.3.6}$$

where $\dot{Q}_{\text{cond}}$ is the heat transfer rate through conduction, k is the thermal conductivity of the material, A is the cross-sectional area of the material, T is the temperature, and dx is the distance over which the temperature gradient is measured.

Convection is the transfer of heat from a surface to a fluid medium, such as air or water. This concept is the most important for modeling and predicting the performance of a TMF test machine as it is the main mechanism for cooling the

specimen in a typical system. The rate of heat transfer through convection is given by Newton's law of cooling:

$$\dot{Q}\text{conv} = hA(T_s - T_\infty) \tag{2.3.7}$$

where $\dot{Q}$conv is the heat transfer rate through convection, h is the convective heat transfer coefficient, A is the surface area, T_s is the surface temperature, and $T\infty$ is the fluid temperature.

The convective heat transfer coefficient, h, is dependent on the properties of the fluid, the properties of the surface, and the velocity of the fluid. It can found using a computational fluid dynamic simulation, or it be calculated using the Nusselt number, Nu, which is a dimensionless parameter that relates the convective and conductive heat transfer rates:

$$Nu = \frac{hL}{k} \tag{2.3.8}$$

where L is a characteristic length scale of the system, such as the diameter of a pipe or the length of a flat plate.

Radiation is the transfer of heat through the emission and absorption of electromagnetic radiation. The rate of heat transfer through radiation is given by the Stefan-Boltzmann law:

$$\dot{Q}\text{rad} = \varepsilon\sigma A(T_s^4 - T_\infty^4) \tag{2.3.9}$$

where $\dot{Q}$rad is the heat transfer rate through radiation, ε is the emissivity of the surface, σ is the Stefan-Boltzmann constant, A is the surface area, T_s is the surface temperature, and $T\infty$ is the temperature of the surroundings.

In practical applications, all three modes of heat transfer can occur simultaneously, and the overall rate of heat transfer is the sum of the rates of each mode.

Understanding the relative contributions of each mode is important in designing and optimizing the heating and cooling subsystems of a TMF test machine.

2.3.4 ASTM E2368

ASTM E2368 provides several guidelines for performing thermomechanical fatigue tests, the following listed contains a paraphrased list of all applicable guidelines:

1. The test machine must have tension-compression loading capabilities.
2. The test system must be able to independently control both temperature and total strain.
3. The gripping fixtures used to hold specimens must be made from a material that can withstand prolonged usage at high temperatures.
4. The axial deformation in the gauge section should be measured with an extensometer (should classify as B-2 or better). A class B2 extensometer should have a fixed error of strain less than 0.0002 mm/mm.
5. If induction is to be used as a heating device, select a generator with a frequency sufficiently low enough to minimize "skin effects."
6. Temperature shall be measured using thermocouples; direct contact with the test sample shall be achieved without affecting test results.
7. Sampling frequency of data points shall be sufficient to ensure correct definition of the hysteresis loop. Different data collection strategies will affect the number of data points per cycle needed.
8. Relative humidity controlled if there is an effect. Carefully monitor and report.
9. Test specimen geometry should be measured in at least three different locations to an accuracy of 0.0125 mm (0.0005 in.) or better.

10. The specimen should be loaded into the test machine without subjecting it to damaging forces, and care shall be taken not to scratch any of the gage section surface.

11. The maximum allowable axial temperature gradient over the gage section at any instant within the cycle shall be the greater of: ± 1% * Tmax K or ± 3 K. Basically, achieve uniform axial temperature over the gauge section. A pyrometer may be justifiable to ensure this.

12. The axial temperature gradient should be measured and adjusted with the specimen at zero force prior to the commencement of thermomechanical loading.

13. Temperature-induced thermal expansion strain should be actively compensated during the test.

14. The mechanical strain cycle shape shall remain constant throughout the duration of the test.

15. Both mechanical strain and temperature should remain cyclically constant and synchronized throughout the test duration. No cumulative error is permitted.

16. The temperature value used in assessing temperature/mechanical strain phasing shall be the feedback (actual) value measured in the gauge section.

17. The specimen temperature and total strain shall be monitored during the test.

18. The test is terminated when the conditions for the selected end-of-test criterion (specimen separation, tensile force drop, or microcracking) are fulfilled.

19. The elastic modulus, as a function of temperature, may be measured, depending on needs.

20. The specimen is thermally cycled until the state of dynamic temperature equilibrium is reached. Recorded temperature compensation should be checked by running the specimen in strain control at zero mechanical strain and monitoring force.

21. The mechanical component of loading should be gradually ramped to its minimum absolute value such that it is reached at an appropriate temperature in the thermal cycle.

2.4 Previous Work

The following subsections outline previous work which is adjacent to the goals of this study but do not fill the intended knowledge gap that existed before this study.

2.4.1 Inconel 718 Material Behavior during TMF

This study presents an experimental analysis of Inconel 718 under TMF and isothermal fatigue test conditions. Deng et al. performed experimentation mechanically cycling Inconel specimens at isothermal conditions of 350 and 650 degrees Celsius, and also with in-phase and out-of-phase thermal cycling between the two aforementioned temperatures. The four cycling modes are displayed in Figure 2.2. A summary of the findings are as follows. It was determined that increased temperature at isothermal conditions increased the degradation rate, and that TMF further increased that rate in both phase-types. Peak tensile stresses under isothermal and TMF fatigue conditions are different and the values correspond to the fatigue lifetime. [7] Finally, the fatigue life under TMF condition can be predicted by the hysteresis energy heating model including consideration of mechanical and thermal strains. The hysteresis loop models used to predict strain conditions is displayed in Figure 2.3. This work is relevant to the test type which is intended to be performed by a TMF test machine and establishes an unbiased baseline to evaluate the performance parameters of such

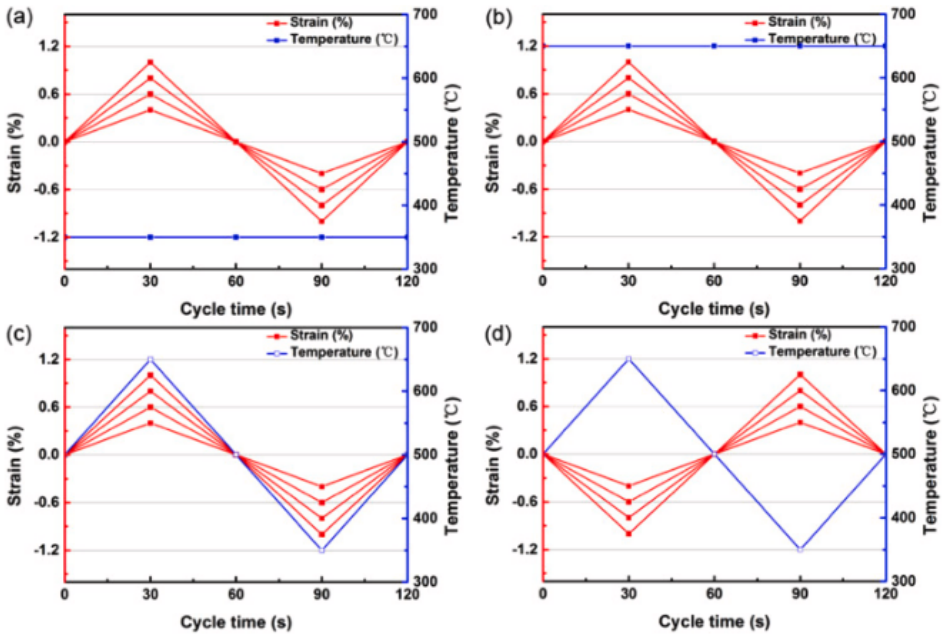

Figure II.2: Fatigue Test Parameters [7]

a machine. This work does not complete the knowledge gap in the design of the machine itself.

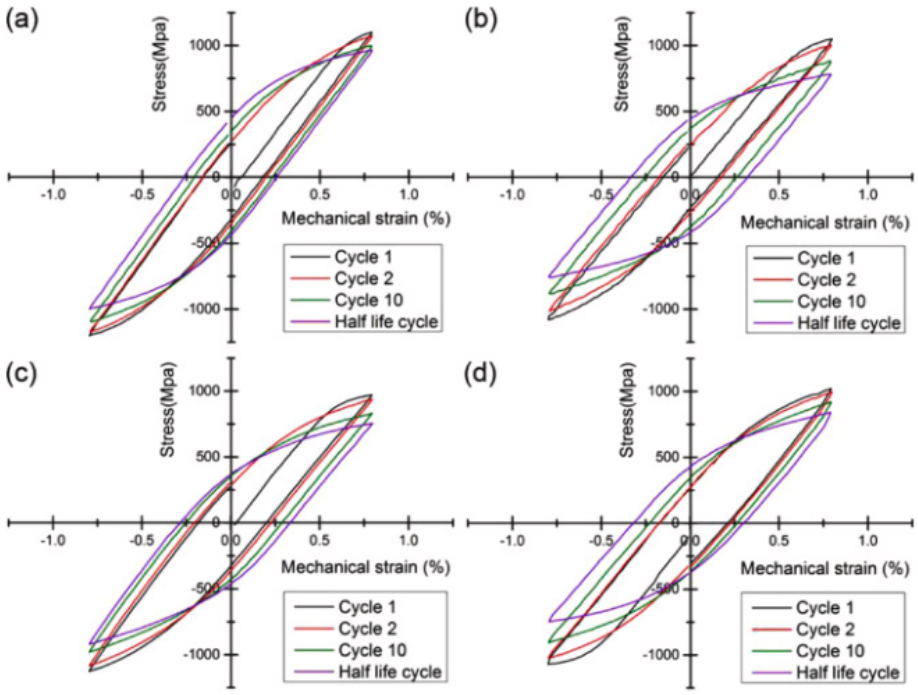

Figure II.3: Hysteresis Heating Loops [7]

2.4.2 Thermal Gradients

This paper presents work done based on the recommendations of a previous group that provided an optimal thermal range to use during TMF testing tubular specimens to determine the maximum acceptable thermal gradient (displayed in Figure 2.4). The study proposes to use FEA to predict thermal gradients encountered during

Gradient type	Absolute range	Relative
Axial	±10 °C	±2% (in °C)
Radial	±5 °C	±1% (in °C)
Circumferential	±5 °C	±1% (in °C)

Figure II.4: Thermal Gradient Parameters [10]

a TMF test. An error estimator is developed to estimate the FEA error due to the ignored structural thermal gradient to further confirm the the thermal range recom-

mendations provided by previous work. Maurel et al. go on to describe the difficulties of evaluating and predicting non-linear behavior law identification experienced during TMF testing. "Thermal and strain field measurements could certainly improve the test monitoring, but could not be seen for the time being as an efficient and intensive industrial tool". [10] Both numerical and experimental works allow to explain the geometric instabilities of the relevant tubular specimen. The most relevant takeaway from this study is the acceptable thermal gradients determined in the axial, radial, and circumferential directions. These gradient tolerances were determined by the error estimator created earlier in the study which is based on an energetic analysis of the specimen and thermal loading conditions. The ranges (in Figure 2.4) found align with the recommended ranges provided by the previous work group. It was also qualitatively determined that at low temperature gradients, the circumferential gradient was the most detrimental to behaviour identification robustness, displayed in Figure 2.5 below.

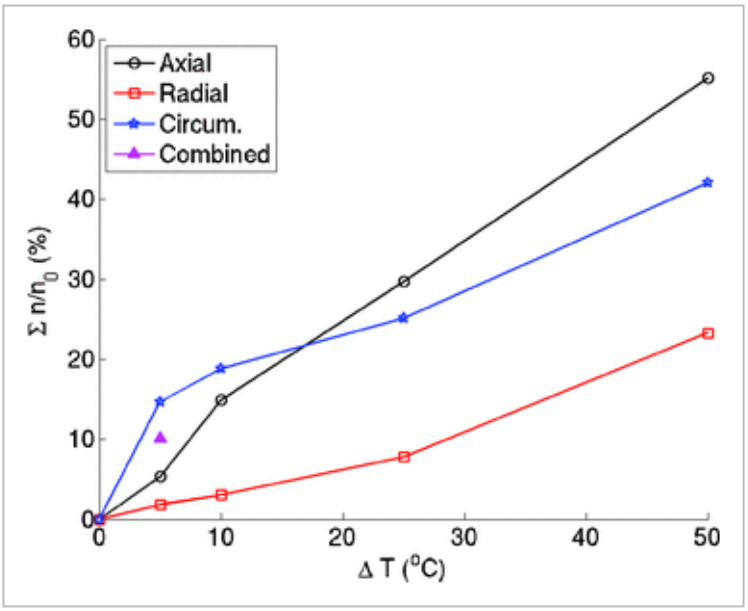

Figure II.5: Error Estimator with Thermal Gradient [10]

2.4.3 Induction Heating

Patil et al. introduced an analytical study investigating the effect of various coil shapes on the induction field distribution, and subsequently temperature distribution, along a specimen being heated.[14] COMSOL Multiphysics FEA solver is utilized to obtain these predictions. In this study four coil geometries (Displayed in Figure 2.6, are analysed: classic, conical, square, and oval.

Work was performed to obtain current densities within the coils as well as induction field distribution between the coil and work specimen. Predictions were also obtained as to the current density within the coil based on the shape of the coil alone. This finding is informative to qualitative predictions on optimal coil shape for a certain intended work specimen. Figure 2.6 illustrates the expected current densities.

The final relative finding is the temperature distribution along a specimen for each coil shape. These distributions were obtained based on the result of energy dissipation within the wall of a hollow work piece. It can be noted from Figure 2.7 the

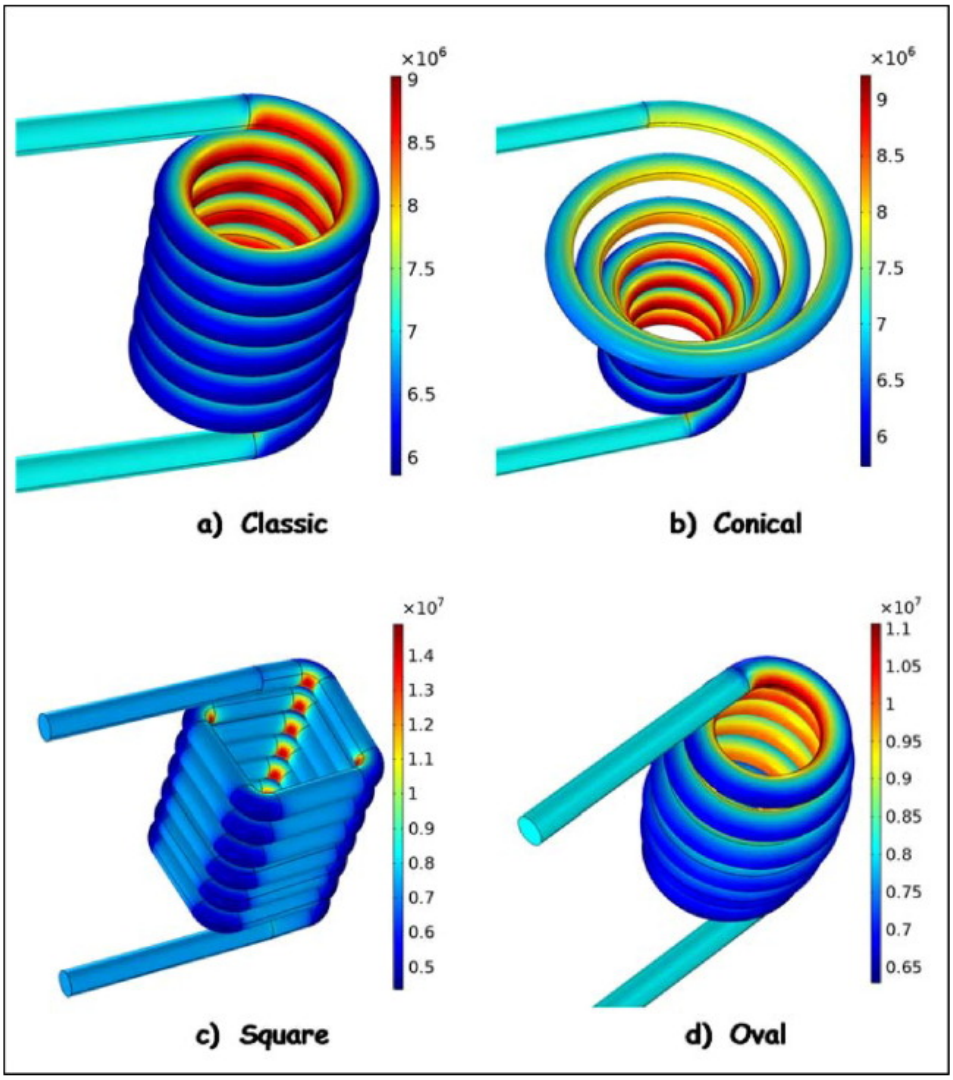

Figure II.6: Induction Coil Current Densities [14]

classic and square coil shapes have the most symmetrical and centered temperature profiles, while conical shape is more highly concentrated on the lower half and the oval is asymmetrical and concentrated more on one end. These analytical findings are informative to the design of an induction coil for any purpose, but more importantly are relative to the design of multiple coils for a TMF system that is intended to support a wide range of test specimen geometries.

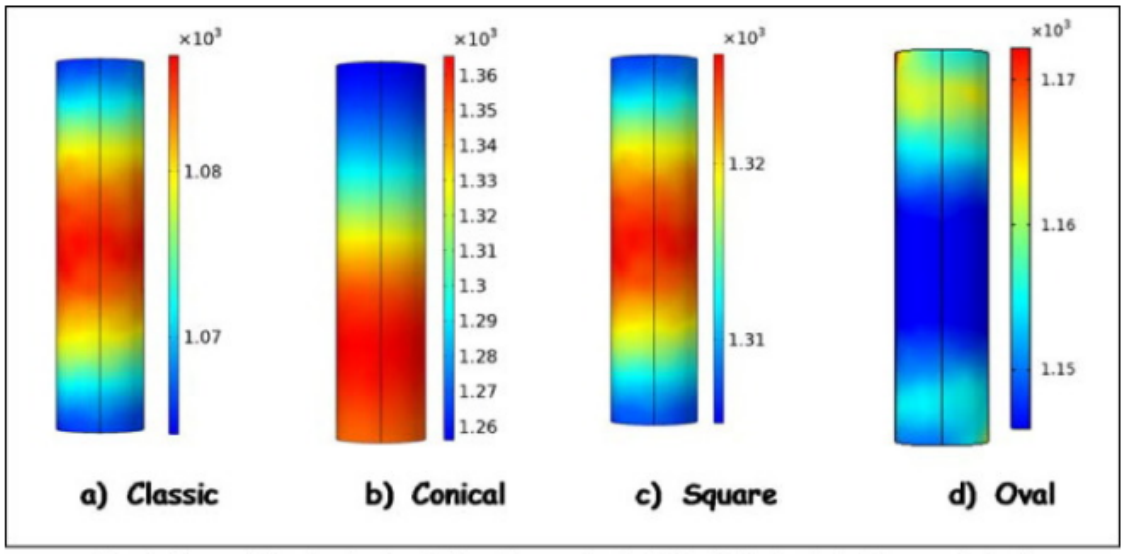

Figure II.7: Induction Coil Temperature Distributions [14]

2.4.4 Temperature Effects on Emissivity

Greene et al. performed a study to evaluate how emissivity changes with respect to temperature for a specific material - INC718. Emissivity is an important factor to consider when calibrating infrared pyrometers, as it can significantly affect the accuracy of temperature measurements. Infrared pyrometers work by measuring the amount of infrared radiation emitted by a material and using this information to calculate the material's temperature. However, the amount of radiation emitted by a material is dependent on its emissivity - a measure of how efficiently the material radiates energy.

The researchers claim INC718 is a nickel-based superalloy that is commonly used in high-temperature applications such as gas turbines, aerospace engines, and nuclear reactors. The material has a complex microstructure, which makes it difficult to accurately determine its emissivity as a function of temperature.

To address this issue, the researchers conducted a series of experiments to measure the emissivity of INC718 at various temperatures. They used a two-color pyrometer to measure the material's radiance at different wavelengths, which allowed them to

calculate its emissivity. The experiments were conducted in a controlled environment to minimize any external factors that could influence the results. The study findings include that the emissivity of INC718 varies significantly with temperature, with a maximum value of around 0.4 at temperatures between 600 and 700°C. They also observed that the emissivity decreased as the temperature increased beyond this range, reaching a minimum value of around 0.2 at temperatures above 1000°C. These findings highlight the importance of accurately determining the emissivity of materials at different temperatures in order to obtain accurate temperature measurements using infrared pyrometers. Figure 2.8 illustrates the relationship developed during the study between actual temperature and observed temperature over the observed temperature range.

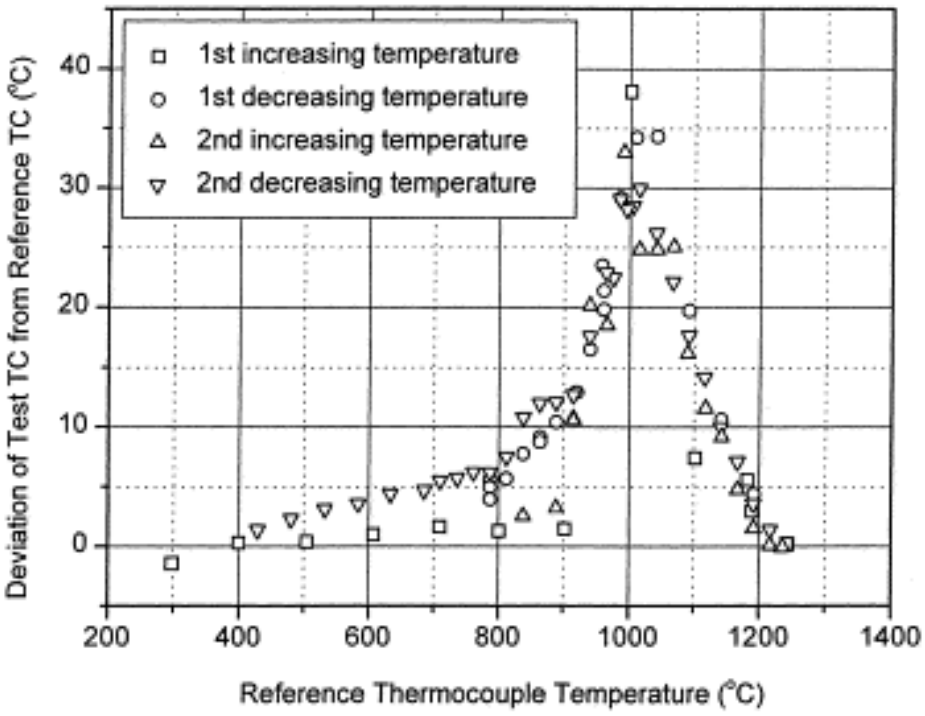

Figure II.8: Emissivity Correlation for INC718 [8]

In addition to the experimental work, the researchers also developed a theoretical model to predict the emissivity of INC718 based on its microstructure and composi-

tion. The model takes into account factors such as the material's grain size, phase distribution, and chemical composition, and was found to provide a good approximation of the experimental results. This model could be useful for predicting the emissivity of other nickel-based superalloys with similar microstructures.

This study provides valuable insights into the emissivity behavior of INC718 and highlights the importance of accurately determining emissivity in order to obtain accurate temperature measurements using infrared pyrometers. The experimental and theoretical approaches used in the study could also be applied to other materials with complex microstructures and compositions. Most importantly, the study illustrates how emissivity can change with temperature for both oxidized and un-oxidized Inconel 718, and the importance of performing sensor calibration before beginning work with a pyrometer.

2.4.5 Thermomechanical Fatigue Modeling

Zaletelj et al. present a study focuses on the evaluation of endurance of machine parts exposed to thermomechanical fatigue (TMF) through numerical methods.

The authors presented three different numerical methods: Chaboche, Skelton, and Prandtl operator approaches, which assume a stabilized elastoplastic response and do not include creep. The properties, weaknesses, and possible improvements of each model are also studied. The non-linear kinematic hardening model is used to model the stabilized curves in the framework of time-independent plasticity. Temperature influence is also considered in all models through parameter dependence and changing temperature versus time.

The study compares the numerical results obtained from each model with the experimental TMF cycles for different load conditions, and their accuracy is evaluated. The comparison of the results of different numerical models shows good agreement with the observed values. However, the ratcheting effect, which is difficult to elimi-

nate, can cause higher deviation from the predicted results.

The Chaboche model shows the ratcheting effect, especially when the mean-stress is significantly lower than the stress amplitude. The classical Chaboche constitutive equations do not describe the ratcheting effect correctly. However, a set of modified kinematic rules is introduced to eliminate ratcheting. The non-linear kinematic model greatly over predicts ratcheting when its identification is performed for normal monotonic and reversed cyclic conditions. A non-linear kinematic model with a threshold is proposed in [19] as the best choice to describe both normal cyclic conditions and the ratcheting condition.

The authors concludes that the Prandtl operator approach is preferred over the Chaboche model due to the ratcheting effect causing higher deviation from the predicted results. The precise results of the Chaboche model require consideration of the correction of the ratcheting effect.

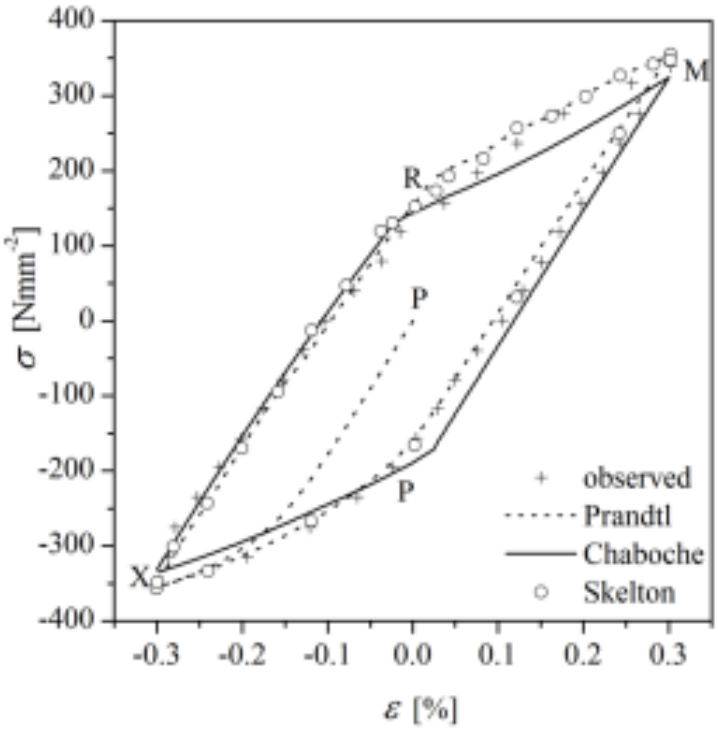

Figure II.9: TMF Model Hysterisis Loops [19]

Figure 2.9 shows the comparison of the experimental results (displayed as "observed") with the numerical results of the other models for one TMF cycle type evaluated. Multiple combinations of strain and temperature were selected in a complex test matrix, but the results are relevant only up to the general method and overall observed effects. The ratcheting effect is clearly visible in the figure, indicating the deviation of the numerical results from the experimental results. Figure 2.9 also shows the comparison of the experimental results with the numerical results of the Prandtl operator approach for the same TMF cycle. This displays good agreement between the experimental and numerical results, indicating the effectiveness of the Prandtl operator approach. The modeling findings may be useful to future work and support post-development of a new system, but do not sufficiently complete the need for a versatile experimental apparatus.

2.5 Research Objectives

2.5.1 Objective 1

The first research objective is to design a versatile thermomechanical fatigue test system retrofit kit. This design must be based on the previously listed ASTM E2368 TMF testing standards, and the design will be initially intended for the testing and evaluation of Inconel 718. The system must also be designed to support the evaluation of a variety of aerospace materials with the only limitation being that the material must be ferromagnetic to effectively incorporate an induction heating element. The system must be able to autonomously perform cycling without an operator present through the majority duration of a test. A major aspect of the versatility for a retrofitted design is the ability to adjust the positions of major system components so that the compatibility with a machine is never compromised by conflicting part placement. To meet these criteria, the design will inherently consist of an open ar-

chitecture to allow for the substitution of low-cost minor components when necessary and allow for the testing of a high variance of test specimen geometries and lengths.

2.5.2 Objective 2

The second research objective is to analytically evaluate the performance of the system and the ability to synchronize thermal and mechanical loading profiles. Once major components are selected for the design, analytical work must be performed to ensure the system can meet the required thermal and mechanical loading specifications. Additionally, the control system must be evaluated to ensure the two loading profiles can be synchronized by determining the response rates and optimizing control logic to ensure there is no accumulating error over a large number of cycles. The system must also be evaluated to ensure all sensors and heating/cooling components do not impede the other's performance at any point. The system must be evaluated for safety ensuring there is no risk of the induction coil or nearby components overheating during the course of an extended test period.

2.5.3 Objective 3

The final objective is to experimentally validate the ability of the system to synchronize the thermal and mechanical loading profiles as predicted. This will occur in two stages: first, what will be noted as the "tuning" phase, followed by the cycle evaluation phase. Due to the rate of heating being determined by the power supplied to the coil and the cooling rate being determined by the flow rate of air over the specimen, both of these components will be experimentally evaluated to determine the optimal quantities of each for a desired cycle period. Once an array of heating and cooling times- as determined by the previous quantities- is acquired, phase two can begin by determining the accuracy of profile synchronization. This accuracy will be determined by metrics developed that define correlations between the two profiles

and can track what percentage of the total cycle time the profile synchronization is outside of the acceptable tolerance. If needed, the first phase can be revisited to further tune the system components if the initial set of values do not provide acceptable profile synchronization.

CHAPTER III

Design of the Test Apparatus

3.1 System Overview and Specifications

The TMF rig captures all necessary functions vital to performing this kind of testing while at a fraction of the cost of a similar system: costing approximately $15K in material component costs (BOM located in Appendix A). The retrofit is currently designed to be attached onto an MTS 380, the available universal test machine, shown in Figure 3.1. With an independent control system and no necessary interfacing with UTM-specific software, the rig can be attached to any dynamic loading machine of relatively similar size and work space.

The test rig is capable of testing at a temperature range of 68-1800 °F and can support specimens with a gauge section length greater than 0.5 inches. Thermal cycling rates are dependent on the specimen size and material composition and due to the induction heating method can only support ferromagnetic material. The system also utilizes two separate methods for temperature evaluation and verifying an axial temperature gradient with a thermocouple located at either end of the grip-section of the specimen and an infrared pyrometer directed near the center of the gauge section. The control system is composed of an Arduino Uno that is able to interface, read, and control all components throughout testing by following a custom coding protocol. The overall test operates by using the mechanical cycling as an independent preset and actuating all other elements of the system based on the strain read from the extensometer to synchronize the thermal and mechanical loading profiles: i.e.

Figure III.1: MTS 380 Universal Test Machine

providing a strain-controlled test with an active feedback loop as required by TMF testing standard ASTM E2368. An image of the work-area on the assembled test stand is shown in Figure 3.2 and Figure 3.3.

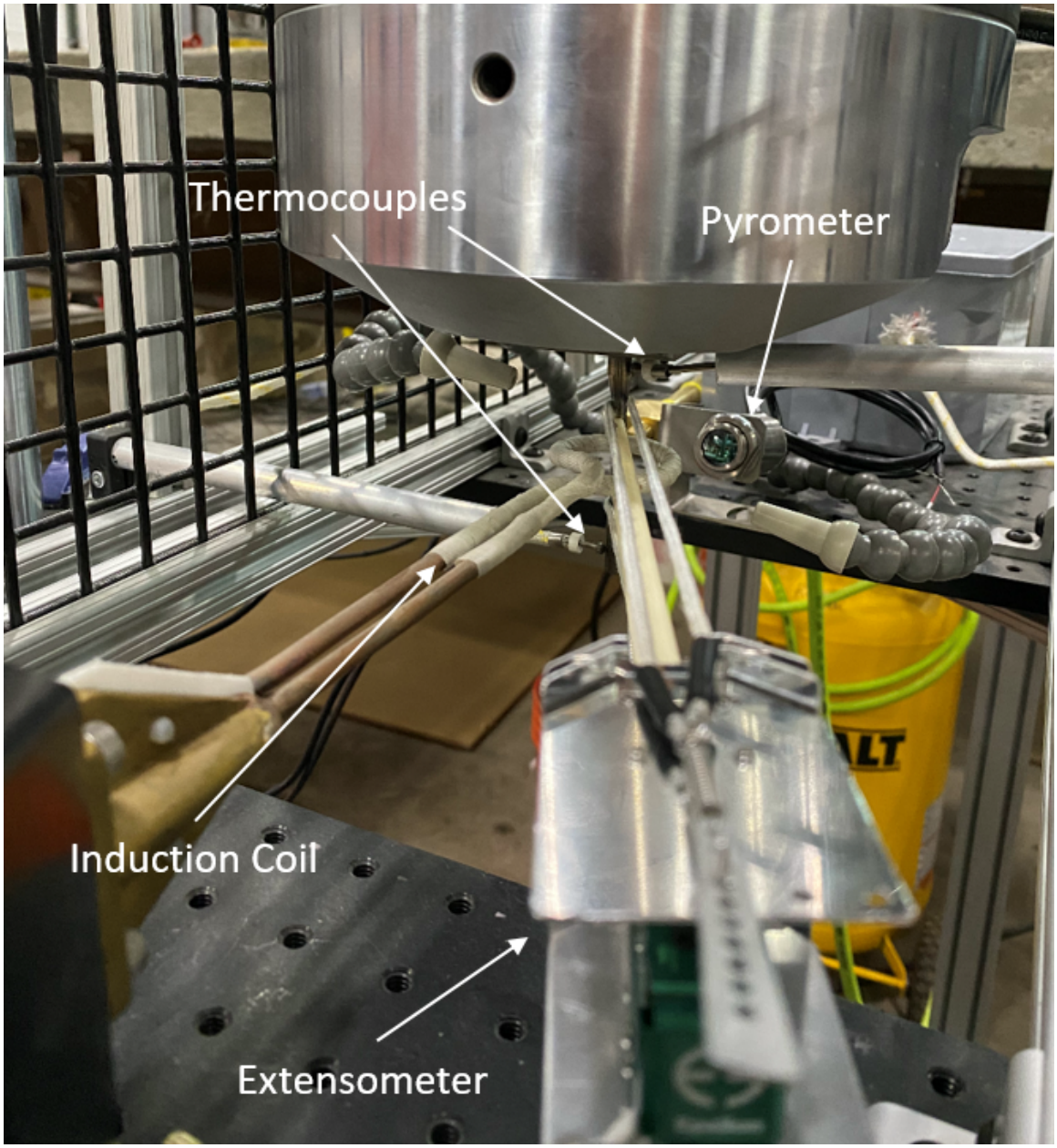

Figure III.2: Assembled Work Area Front View with INC718 Specimen

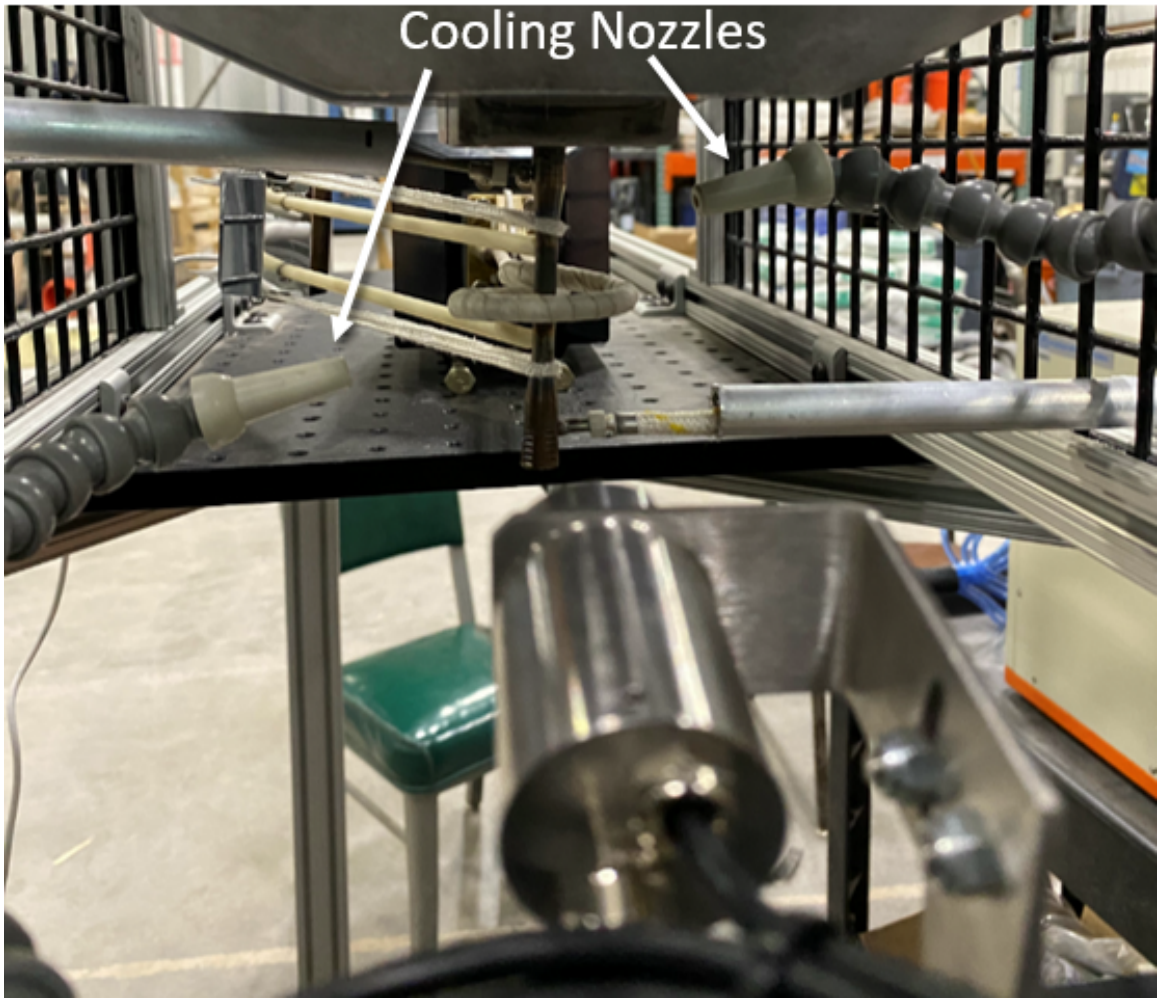

Figure III.3: Assembled Work Area Back View with INC718 Specimen

3.2 System Component Design and Selection

3.2.1 Test Specimen

To begin designing each component of the TMF system, an initial test specimen was selected to optimize the design for ,and to give general size and material characteristic values. This allows for a completed design optimized for a certain material to be later modified within the open architecture to accommodate for a larger range of ferromagnetic materials. The specimen material was selected as the nickel alloy Inconel 718 due to the wide use, especially in areas where thermomechanical fatigue is present such as turbine blades, and documented characteristics. The material is

has high strength and temperature properties making it a good candidate for TMF testing. The specimen size was determined primarily by the UTM's loading capabilites (-100 kN to 100 kN) and secondarily by reducing the diameter to help reduce heating/cooling times and skin effects during the heating process. The specimen was also subjected to LCF testing in work preceding this study. The specimen was designed according to the with a gauge section diameter of 0.2 inches and length of 1.18 inches. A drawing of the specimen is displayed below in Figure 3.4. The speci-

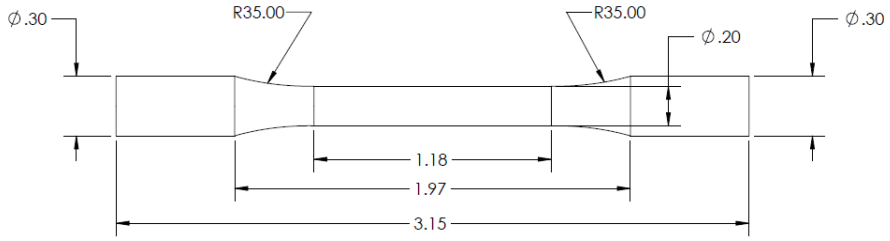

Figure III.4: Test Specimen Dimensions

mens were machined and then precipitation hardened and then polished to a smooth surface finish to more closely align with material properties found in literature. A completed specimen is shown in Figure 3.5.

Figure III.5: INC718 Test Specimen

3.2.2 Structure

The structure which holds all components in necessary place is composed primarily of aluminum T-slot with base plates made from optical bread boards. The structure is free-standing with the two bread boards stationed on either side of the work space

for controller and component mounting. Once assembled, the sides of the stand are clamped to collars attached to the support rods on the sides of the MTS machine. This extra clamping ensures that the structure is stable enough to withstand a normal adult pushing or leaning on it and it does not move especially while a test is being run. A CAD drawing of the overall structure is displayed in Figure 3.6.

Figure III.6: Test Rig Structure CAD

The structure being constructed almost entirely out of T-slot aluminium makes the entire system highly modifiable with the versatility to adjust any part alignment and dimensions. This further allows for a wider range of compatibility with UTM's of varying heights, width's, or horizontal clearances. The only drawback in the structure design is that it requires roughly a square foot of flat ground in front of and behind the UTM to place the base of the structure.

The structure also includes rubber coated aluminium caging on either side of the work area. This is intended to add a layer of safety to the design by preventing a

nearby person to reach a hand or arm into the specimen work area. This cage is also intended to provide space to support additional sensors or observation tools to be mounted safely near the work area without the need to move or adjust any existing components. This mesh guard is displayed below in Figure 3.7.

Figure III.7: Mesh Panel Safety Guard

3.2.3 Mechanical Loading Grips

The grips used for TMF testing are V-Wedge serrated hydraulic grips. The grips are suitable for loading in tension and through-zero to compression. The design of these grips are self-aligning and do not require special calibration during specimen installment between tests. The grips will be located far enough from the induction coil and will not conduct enough heat to cause cooling concerns. Additionally, the grips are rated by the manufacturer to operate at 1000°F within a furnace or other high temperature environments for prolonged periods of time, which further reduces any concern about damaging or melting the grips. The limitation on these grips is they are only suitable for a solid specimen, so that if a tubular specimen is used in

the future, a new set of grips will need to be purchased. The grip is a clamp style and one-half is shown in Figure 3.8 to illustrate the shape and style.

Figure III.8: Hydraulic Grip Style

3.2.4 Induction Heater and Industrial Chiller

The heating system features a 6.6 kW induction heater with an operating frequency range of 500-1100 kHz. The heater can operate at a maximum output power of 2.8 kW, and at this power operates at 750 kHz. The coil is connected to a wand that is in-turn connected to the heater by tubing so that the wand can be mounted in the work area with the heater itself at a safe distance. The coil wand is attached to the optical breadboard with pins so that it is is unable to shift out of place through the duration of a test. The exact heating time the coil can provide to the Inconel specimen is difficult to predict within the necessary certainty, and tuning must be performed before conducting a test to determine exact heating rates and resulting heating period time. The heater also features a custom ordered 1-turn induction coil which has a 1.25 inch diameter. This coil selection will improve heating rates while ensuring no contact between the specimen and the coil at less than a few hundred dollars- so that if further modifications are necessary, or a different diameter specimen is to be tested, a new coil can be purchased and installed easily and at little cost.

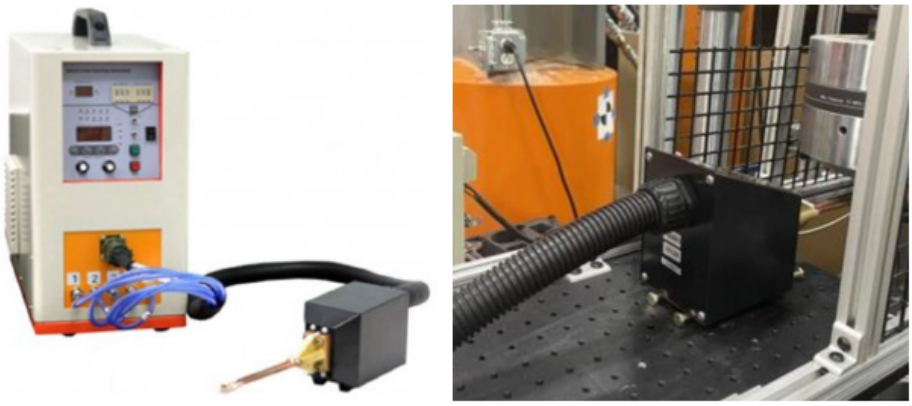

Figure III.9: Induction Heater and Coil Mounting

The heater is fitted with a remote socket and foot pedal to allow for easy actuation of turning the heater off and on, and for implementation onto the TMF rig the remote socket is connected to a relay within the control system instead of a foot pedal to allow for digital control. The front panel of the system displayed in the left image of Figure 3.9 allows for manual input of the operation power and operating modes which do not change through the duration of a test.

The induction heater also requires forced water circulation to cool the system and the coil itself. For safe operation the heater requires flow at 44 psi, 0.8 GPM, and less than 100°C. After initial iterations with both closed and open-loop cooling designs, the decision was made to purchase an industrial water chiller and circulator to ensure there is no issue with overheating. This chiller is produced by the same manufacturer as the heater and is an intended pairing with ability to meet all flow-rate and temperature requirements for sustained heater operation. The chiller will run continuously whether the induction heater power is on or off, and can also automatically detect and maintain the circulating water temperature at the required 30°C through extended periods of use.

Figure III.10: Industrial Chiller Connected to Induction Heater

3.2.5 Air Cooling

Initial back-of-the-envelope estimates provided a rough starting point for the open-loop design of the cooling system and provided a maximum CFM of around 2 would be sufficient to cool the specimen with 1/8 inch nozzle diameters. A 30-gallon air compressor rated at 5.3 CFM (shown in Figure 3.11) was selected as the source of pressurized air. The main benefit of using an compressor is the flow rate can be tuned by adjusting the tool pressure on the compressor itself.

The air compressor outlet hose is connected to a solenoid valve. This enables instant digital actuation of the solenoid valve by the control system sequence. The solenoid is rated for a maximum pressure of 100 psi. Following the solenoid, the flow is diverted into two separate nozzles through a flow manifold. The nozzles selected

Figure III.11: Selected 30-Gallon Air Compressor

are two bend-and-stay air cooling nozzles with an outlet diameter of 1/8 inch. These nozzles are inexpensive, and in the case of a larger or smaller diameter being required for alternate specimens or arrangement, can be replaced quickly and easily. The solenoid, manifold, and nozzles are displayed below in Figure 3.12.

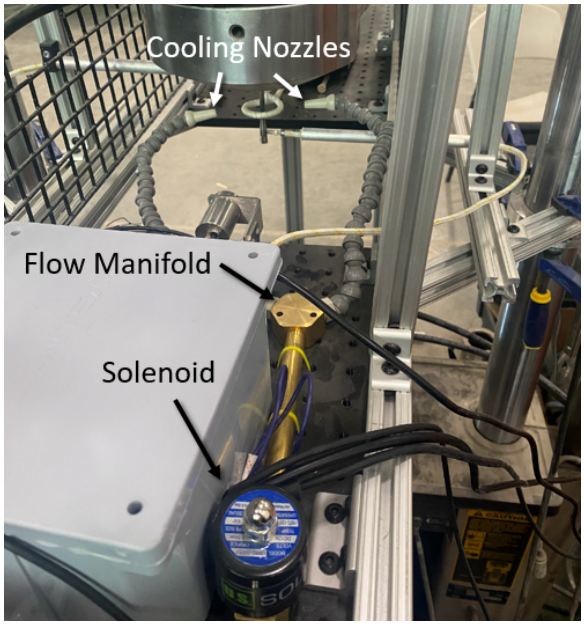

Figure III.12: Air Cooling Components

Cooling times were estimated based on the currently selected components and a the assumed nozzle diameter of 1/8 inch. A Computational Fluid Dynamics (CFD)

study was performed to estimate the convective heat transfer coefficient for a similar nozzle size and flow velocity of 259ft/s with room temperature air. The CFD system setup is shown below in Figure 3.13. This study did not utilize the same number of cooling nozzles as the designed system, but was determined to provide a good estimate for expected values. From this study the convective heat transfer coefficient was determined to be 309 $W/(m^2 * K)$.

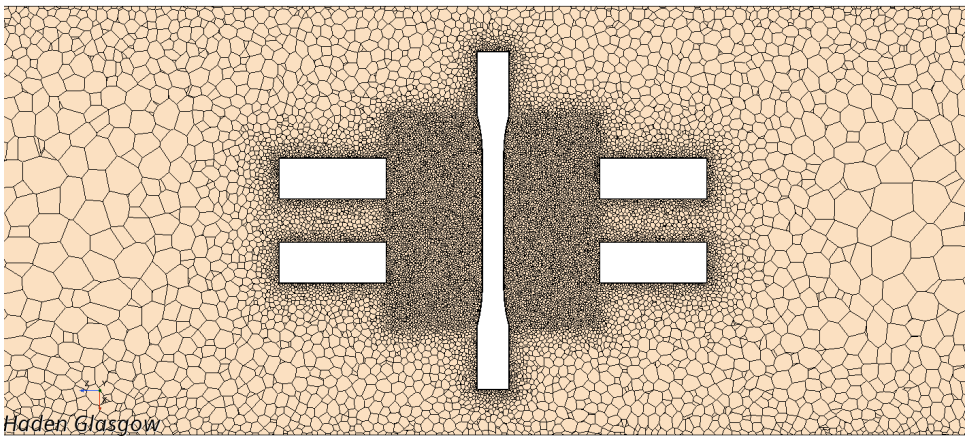

Figure III.13: CFD Study Setup

It is expected that the radiation and convection heat transfer rates will vary with specimen temperature over the course of the cooling period. A relationship was created to predict the average heat transfer rate over the total change in specimen temperature. Equations 2.3.7 and 2.3.8 are used to calculate the heat transfer rate at each temperature value. The resulting plot of heat transfer rate vs. temperature is displayed in Figure 3.14. To simply the cooling assumption due to the nearly linear nature of the combined heat transfer values, an average of 186 W was calculated and used as the cooling rate prediction. Using equation 3.2.1 below and the previously found average heat transfer value of 186 W, the time to coil the specimen from 1600°F to 649°F is estimated to be 18 seconds.

$$t = \frac{m * c_p * (T_f - T_i)}{\dot{Q}} \tag{3.2.1}$$

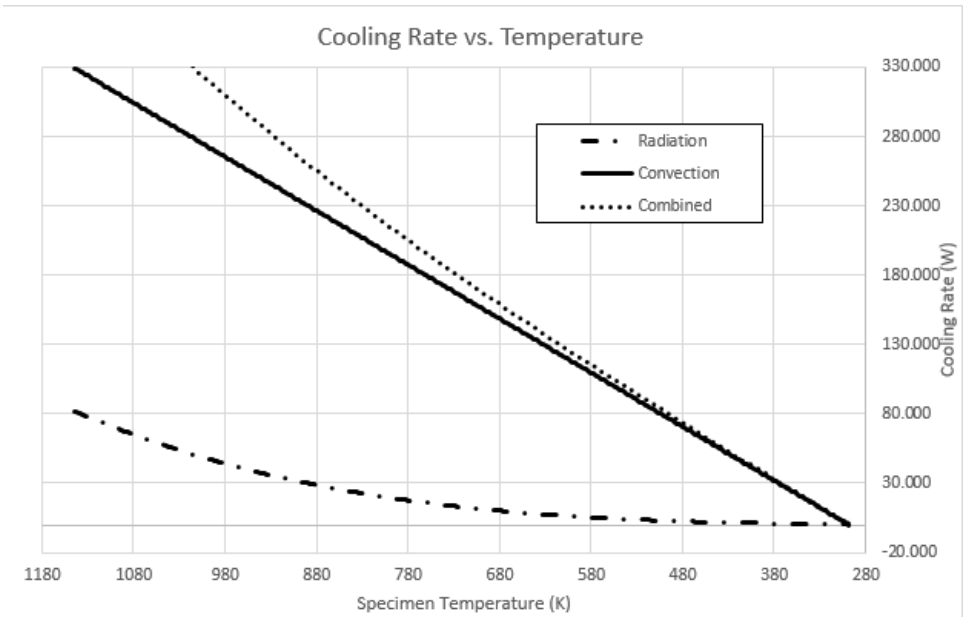

Figure III.14: Heat Transfer Rate Predictions

The other concern with the cooling system is the inability to monitor and actively minimize a thermal radial thermal gradient within the specimen. Future work may ideally consist of a hollow specimen where air can be directed up through the center to further reduce cooling times while also reducing the risk of an accumulated radial thermal gradient. However for the current system design, the size of the test specimen is predicted to be small enough and have a high enough thermal conductivity that the risk of a radial or axial gradient is small enough that a large-scale modification of the system to accommodate for a hollow specimen is outside of the scope and budget of this study. It is recommended that materials tested in the future with a lower thermal conductivity be verified that the gauge diameter is sufficiently small.

3.2.6 Sensors and Data Acquisition

ASTM E2368 calls for thermocouples placed outside of the gauge section to monitor specimen temperature during the course of the test. This standard does not specify the type or attachment method of the thermocouples, and also calls out no specification to verify temperature at the axial center of the gauge section. Following this

guideline, two K-type thermocouples were selected. these sensors are contact based, as opposed to welded or ribbon type, and must be secured to the specimen with either tension or a compression fitting. To achieve this, two aluminium tubes are connected to the structure on either side of the specimen and the thermocouple sensors are fed through the tube. The sensors are fitted in the tubes, and this arrangement provides adequate compression to sustain contact with the specimen due to the stiffness of the thermocouple wires. Many systems utilize thermocouples that are spot-welded to the test specimen, and while this may have some benefits of reduced response time or increased accuracy, having to remove and re-weld thermocouples to the specimen for every new test has a large impact on the reusability and sustainability of the system. Therefore, the current configuration of compressing the thermocouples to the specimen surface is the more versatile and sustainable alternative. The arrangement is displayed below in Figure 3.15. The thermocouples also utilize ceramic insulation to protect from the radiant heat and induction field. Both thermocouples are ungrounded to avoid creating a grounded loop short circuit when they are both connected to the conductive Inconel specimen- an issue that was discovered during the early phases of testing.

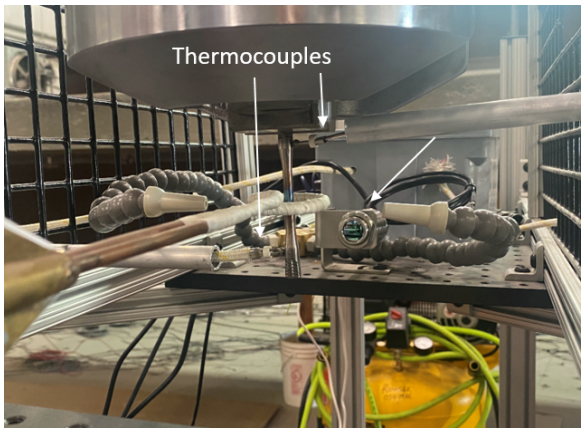

Figure III.15: Thermocouple Arrangement

To monitor and verify temperature agreement with the thermocouples, an infrared

pyrometer was selected. The pyrometer will allow for an additional data point, and also further monitoring to ensure there is minimal temperature gradient between the center and ends of the specimen. The pyrometer, however, requires an additional step before testing can ensue due to the changes in emissivity as the specimen is heated. Emissivity calibration must be performed for every new material that will be tested with the system. Calibration can be achieved by placing the specimen in a controlled heating environment with known temperatures (such as a high-temperature furnace), and taking measurements of the material with the pyrometer [at the same distance from the specimen that it would be measuring on the test rig] at several increments within the intended thermal loading range. Calibration can be used to develop a relationship between the observed temperature provided by the pyrometer and the actual temperature of the specimen. The relationship can then be used in the post-processing of test data to reveal accurate temperature measurements. For the purposes of the current study and validating the ability to obtain useful data, as well as the benefit of using a well documented material like INC718, the pyrometer is calibrated for emissivity based on a relationship developed by researchers in [**?**]. The pyrometer will log all data to a separate file through the course of the test where it will later be corrected for emissivity changes. The data from the pyrometer is not used in the active control loop of the control system, and will only be used in post-test analysis of the specimen temperature profile. Therefore, the pyrometer does not need to interface in any way with the control system code logic.

The selected pyrometer is an Omega IR transmitter with MODBUS compatibility that allows for data transmission over USB to the associated Omega sensor software. The Omega software can also log all data the pyrometer captures automatically, which simplifies the set up and test procedure. The sensor has a temperature range of -40°F to 1832°F with an accuracy of $\pm 0.5\%$. The pyrometer also has an inverted conical focal range, shown in Figure 3.16. To obtain a focal spot diameter of equal to the specimen

gauge section diameter of 0.2 inches, the pyrometer is placed 3.9 inches from the specimen. To align the pyrometer with the specimen gauge section, a person's hand or other material that is higher temperature is placed directly behind the specimen, and removed. The pyrometer temperature readout is an average over the entire 0.2 inch diameter focal point. If there is any temperature increase observed between the material behind and not behind the specimen, the pyrometer is misaligned and is then adjusted according to whether the material behind the specimen affects the observed temperature when only visible on the left or right side of the specimen. The magnitude of this temperature fluctuation also informs how far from perfectly centered the pyrometer focal point is on the specimen. This process is repeated until there is no temperature change when the material is placed behind the specimen. The same process can be performed for vertical alignment by placing the material in front of the specimen and moving it upwards along the specimen until there is a temperature increase. This determines the bottom edge of the focal point, and therefore where the center of the focal point is located from the known diameter.

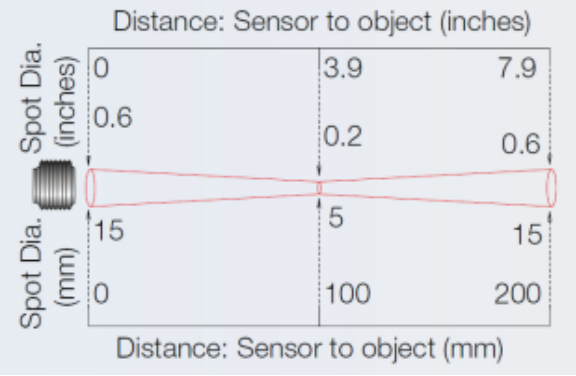

Figure III.16: Pyrometer Focal Range

To create a strain controlled test and serve as the interface between the mechanical loading and all other system operations, a high-temperature self-supporting axial extensometer (Epsilon Model 3448) was selected. The extensometer is also designed to operate near an induction field so there will be no concern with unintended heat-

ing. The mounted extensometer can be seen in Figure 3.2, offset from the induction coil and unobstructed by all other system components with a standoff distance of approximately 10 inches, displayed in Figure 3.17. The extensometer utilizes ceramic standoff rods and is intended for use within or near an induction field. The extensometer also is capable of operating attached to a specimen with temperatures up to 2192°F. This device also meets the ASTM E2368 standard by classifying as class B-1, where B-2 or better is required. The class of extensometer is primarily a classification of the accuracy less than a certain fixed error strain.

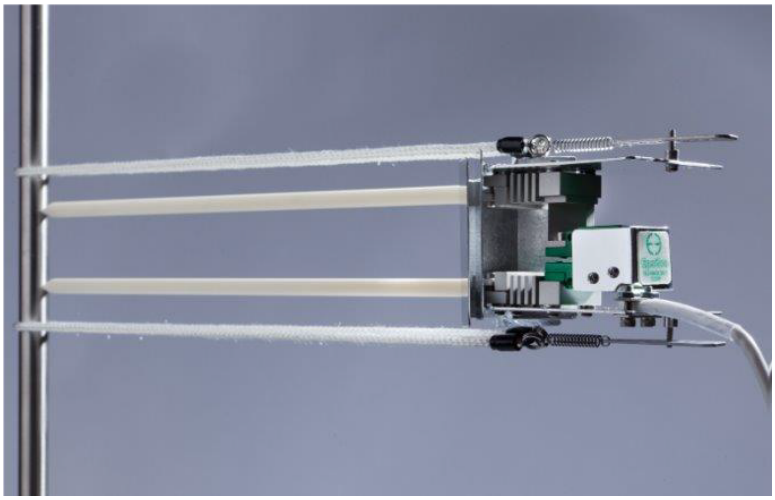

Figure III.17: Epsilon Model 3448 Axial Extensometer

The tips of the ceramic rods which are in contact with the specimen provide several chisel-style tips that ensure the rods will not slip or move in any unintended fashion during the course of the TMF test. The available ceramic tips are displayed in Figure 3.18, and the current tip in use is the "straight chisel" which are suitable for flat and round specimens. If future work determines the extensometer is not centering or attaching properly to the specimen, the "vee chisel" tips can be acquired and equipped from the manufacturer.

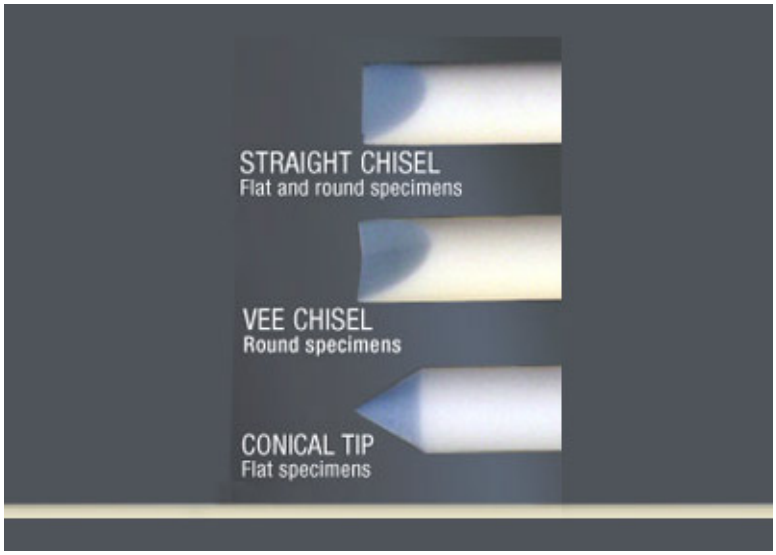

Figure III.18: Extensometer Ceramic Rod Tip Styles

3.2.7 Control System Overview and Data Acquisition

The control system is centered around an Arduino Uno which is connected to a laptop. The Arduino has been connected and can actively take readings and distribute controls to all necessary elements of the system. The signals are captured by the DIGITAL pins on the top of the Arduino UNO. These signals were then used to turn on and off relays connected to the DIGITAL pins as well. The extensometer would be read by the Arduino Uno to gather its information as the mechanical process is independent of the heating and cooling cycles. The heating and cooling cycles need to be synchronized with the mechanical process by reading the extensometer's maximum and minimum displacement data and relating that data to the heating and cooling cycle of the integrated components.

Connected to the DIGITAL pins is the MAX31855 breakout board through header pins. This board was used to interface the small voltages read from the thermocouples by the terminals into readable units for the Arduino and user through the serial monitor. The board has a logic 0 range of –0.3 to +0.8 Volts and a logic 1 range of 2.1 to the Vcc (value of the micro controller output) plus 0.3 Volts. The device

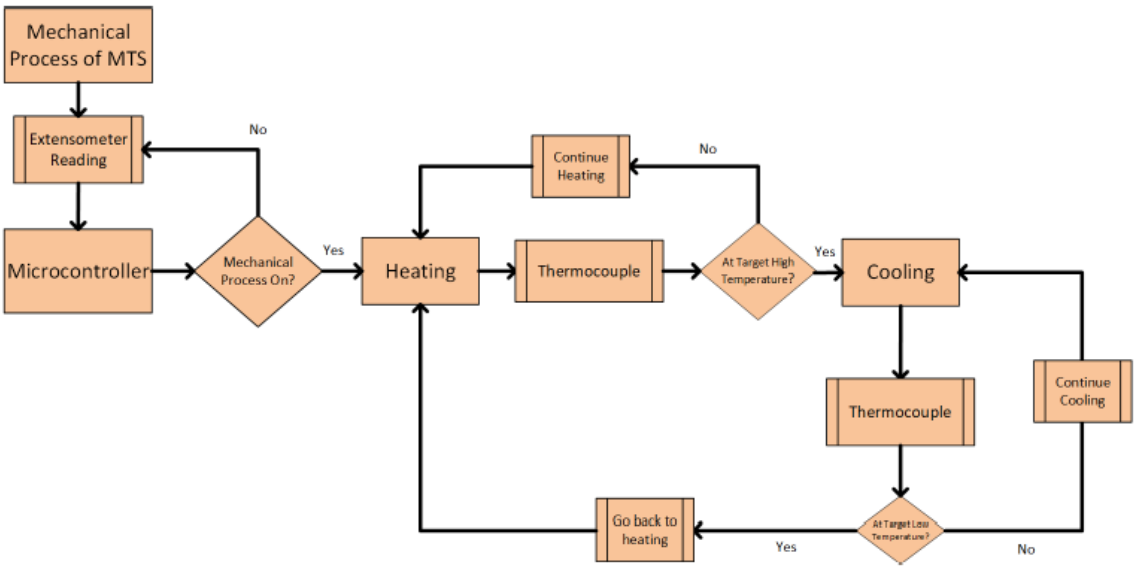

Figure III.19: Preliminary Control System Flowchart

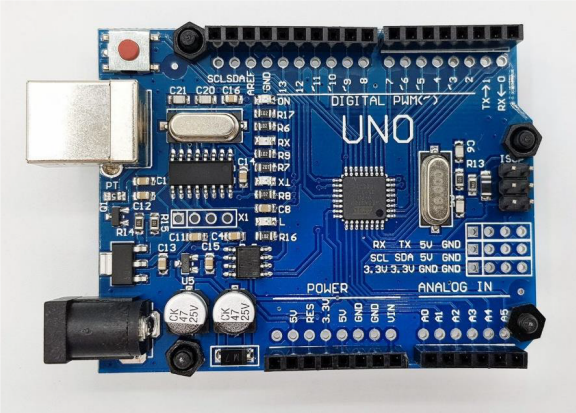

Figure III.20: Arduino Uno Micro Controller

also detects if there is a fault within the thermocouple such as a short circuit or if there is a loose connection between the thermocouple junction and the MAX31855 board. The board communicates with the micro controller through SPI which is a synchronous serial communication interface.

```
void setup() {
  Serial.begin(9600);

  while (!Serial) delay(1); // wait for Serial on Leonardo/Zero, etc

  Serial.println("MAX31855 test");
  // wait for MAX chip to stabilize
  delay(500);
  Serial.print("Initializing sensor...");
  if (!thermocouple.begin()) {
    Serial.println("ERROR.");
    while (1) delay(10);
  }

  Serial.println("DONE.");
}

void loop() {
  // basic readout test, just print the current temp
   Serial.print("Internal Temp = ");
   Serial.println(thermocouple.readInternal());

   double c = thermocouple.readCelsius();
   if (isnan(c)) {
     Serial.println("Thermocouple fault(s) detected!");
     uint8_t error = thermocouple.readError();
     if (error & MAX31855_FAULT_OPEN) Serial.println("FAULT: Thermocouple is open - no connections.");
     if (error & MAX31855_FAULT_SHORT_GND) Serial.println("FAULT: Thermocouple is short-circuited to GND.");
     if (error & MAX31855_FAULT_SHORT_VCC) Serial.println("FAULT: Thermocouple is short-circuited to VCC.");
   } else {
     Serial.print("C = ");
     Serial.println(c);
   }

   delay(1000);
}
```

Figure III.21: Example Operation Code

To control the heater and the solenoid valve with an electrical signal, there are relays (shown in Figure 3.22) to swap between on and off states of the components. Two relays were mounted to the side of the Arduino UNO for ease of use and have connections to the solenoid valve and the induction heater remote-control plug-in. In a simple system, the relay connected to the heater switches from Closed (Powered) to Open (No Power) when the target temperature is reached within a hysteresis range and goes back to Closed when it falls below the hysteresis threshold. The solenoid valve relay switches from Open to Closed when the temperature goes above the hysteresis threshold and switches back Open when the temperature falls below the lower limit.

Data acquisition from the extensometer and thermocouples read through the dig-

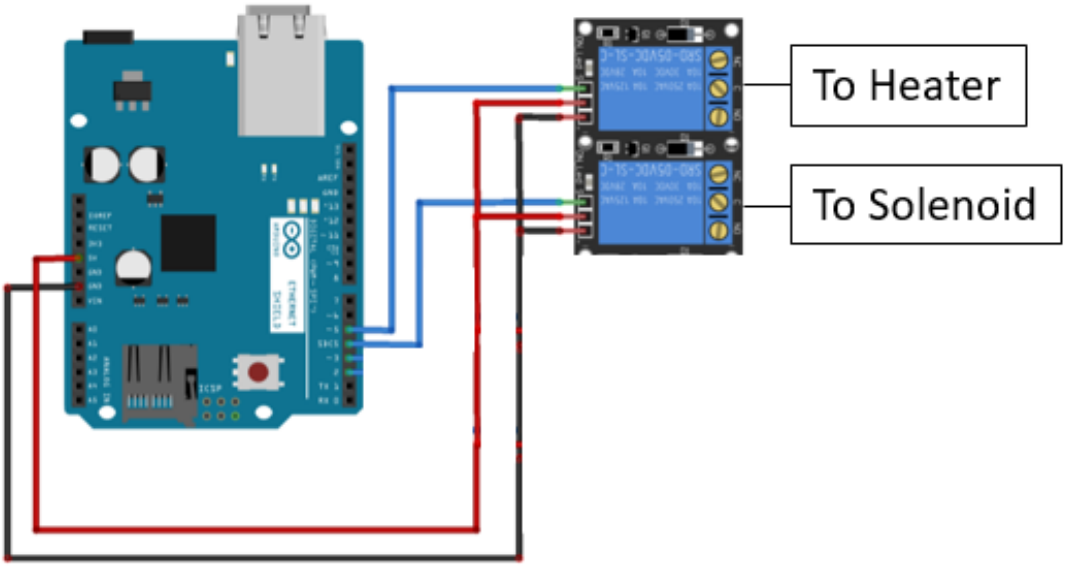

Figure III.22: Arduino Relay Connections

ital and analog pins, respectively, are exported to the Arduino serial monitor (displayed in Figure 3.23) where the data is then extracted from the micro controller to a Microsoft Excel spreadsheet for recording. The Excel spreadsheet utilizes a plugin known as Data-Streamer to extract all data sent to the serial monitor. This data logging process is only for recording and post-processing the temperature and strain data and has no impact on the system active control process.

The control boards and relays are wired and assembled within an electrical enclosure to provide an insulated container for the control components. The assembled enclosure is displayed in Figure 3.24.

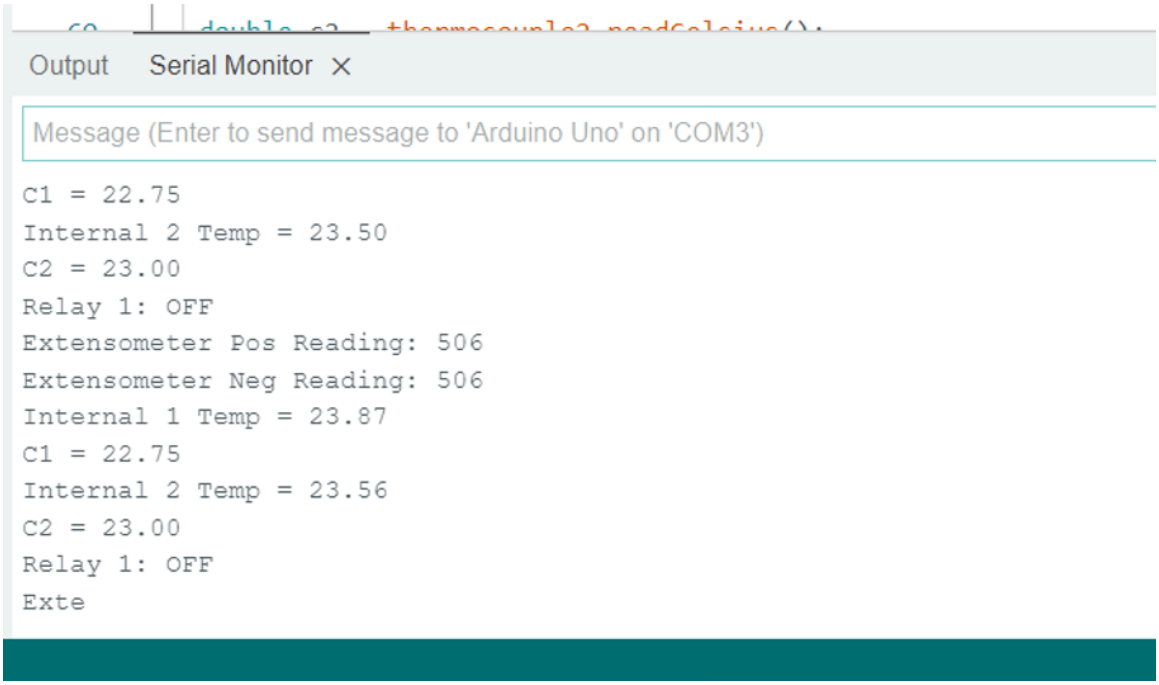

Figure III.23: Arduino Serial Monitor

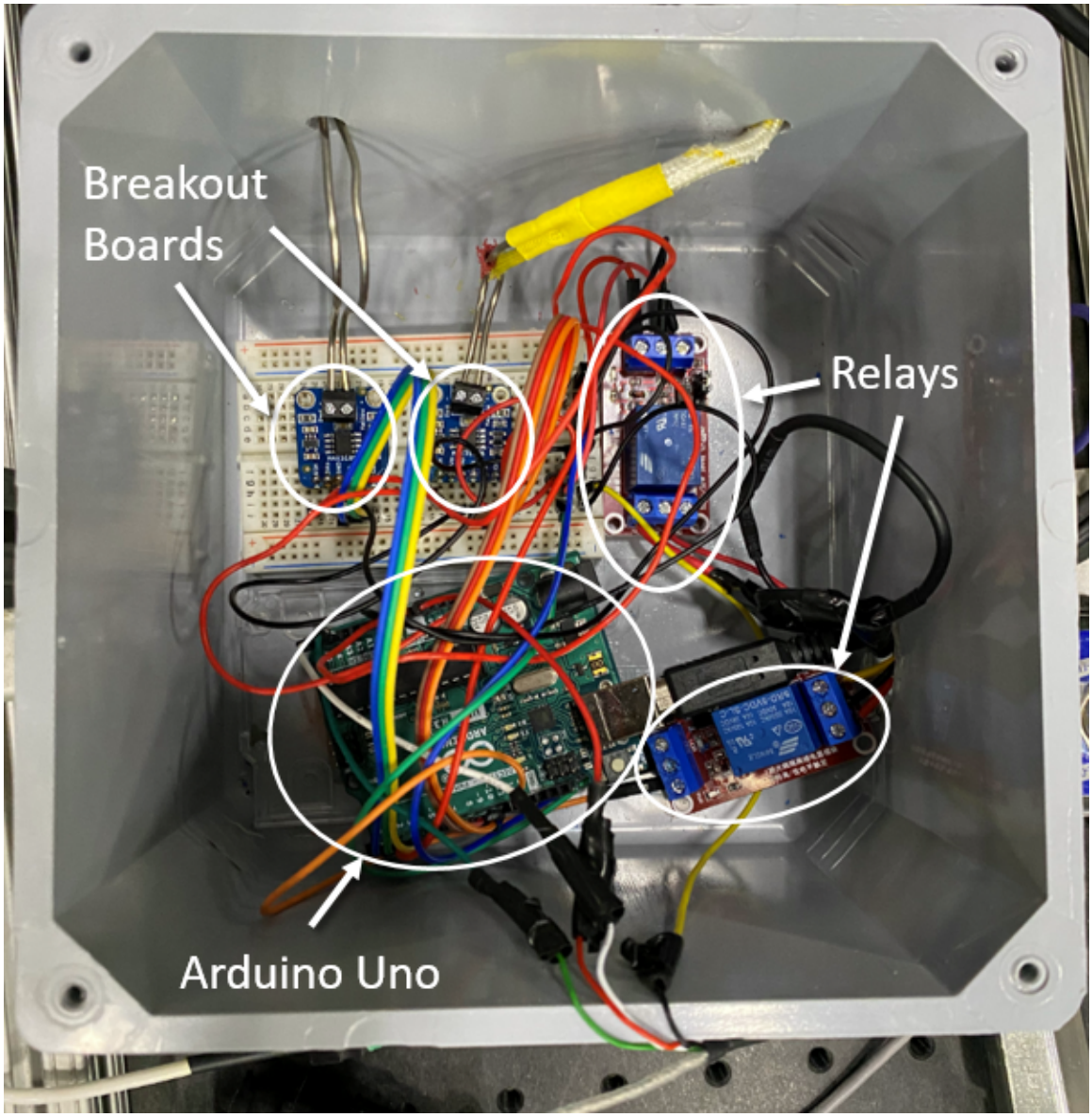

Figure III.24: Control System Enclosure

CHAPTER IV

Testing and Validation

4.1 Phase 1 - Tuning

The first phase of experimental validation of the TMF testing apparatus was intended to evaluate the heating and cooling performance of the system components, as well as verify the ability to monitor temperature with the thermocouples. Induction heater frequencies are typically determined by the specimen gauge section diameter and required heating rate. Small specimens typically require a frequency greater than 50 kHz, and large specimens require a frequency from 10 kHz to 50 kHz [17]. From Initial calculations using the equation for skin depth based on frequency, equation 2.3.3, resulted in an operating frequency of 750 kHz that results in a skin depth of approximately 0.02 mm. The values used in the equation for resistivity and permeability are approximations based on values obtained and used by Sun et al. [17]. This value is only used for an initial estimate to obtain a testing frequency and the operating frequency for each test would be a function of the test conditions and material properties and geometry.

The primary goal of the tuning phase was to obtain relationships between various induction heater operating powers and the relative heating times. The secondary goal is to simultaneously obtain similar relationships between several operating tool pressures and cooling times. This data is intended to inform the operating conditions of the system in the second experimental phase so that the overall cycle time is minimized while not degrading system performance. To perform these tests, a test

matrix was developed with a range of heating power values from 1 kW to 2.8 kW, and a range of cooling flow rates that are directly controlled by the tool pressure of the air compressor, across a range from 25 psi to 75 psi. Ideally, cooling times could be further reduced by increasing the tool pressure above 100 psi, but the solenoid valve used to control the air flow is rated for a maximum of 100 psi. Table 4.1 contains suggested values for the initial tuning test, and example heating and cooling time results.

Table IV.1: Suggested Tuning Test Matrix

Heater Power (kW)	**Heating Time (s)**	**Tool Pressure (psi)**	**Cooling Time (s)**
1		25	
2		50	
2.8		75	

4.1.1 Tuning Control Logic

A set of control code was created to perform the initial testing phase. This control logic was created separate from the code used to run a normal TMF test in experimental phase two. This scheme was created to run testing of a single cycle where the specimen is heated from room temperature to the maximum intended temperature. The beginning and end temperatures are of no consequence as this experiment is only intended to analyze the rates of heating and cooling between the minimum and maximum temperatures of 650°F and 1600°F, and any data outside of this range can be omitted from analysis.

The system operation for the tuning phase is directed towards the completion of a single cycle and not repeated cycling. The flowchart in Figure 4.1 describes the process for this single test. The test begins by initializing the sensors and data collec-

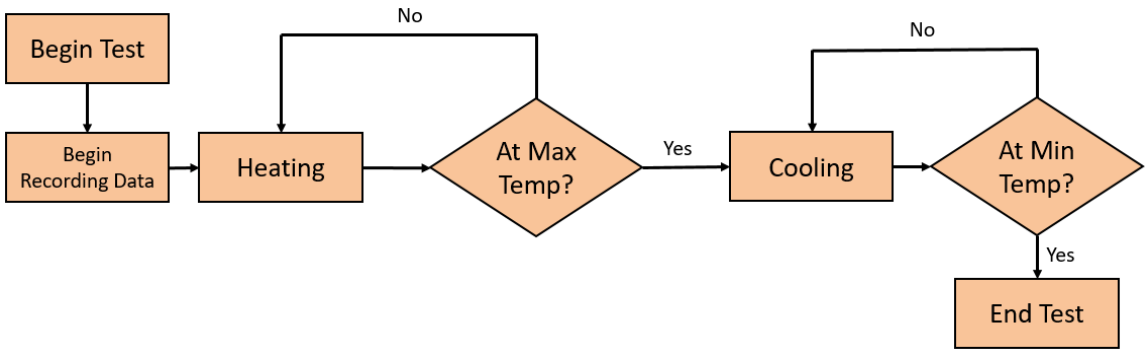

Figure IV.1: Phase 1 Control Flowchart

tion, and beginning to heat the sample. Once the thermocouples detect the specimen has reached maximum temperature, the system actuates the heating component off and the cooling component on. The cooling component will run until the specimen reaches the minimum temperature, and therefore the end of the test. This testing will be completed over the range of heating powers and cooling flow rates by manually changing the operating conditions of the system between each test to obtain all necessary data.

The phase 1 control code was primarily developed to streamline the tuning process, as tuning must be performed before testing every new material and geometry combination to acquire accurate cycle operation and allow for accurate pre-programming of the mechanical loading profile within the UTM software prior to phase two and final testing. Once the operating parameters for the induction heating power and air compressor tool pressure are determined for a certain material/geometry combination, the parameters can be logged into a database, so that if future testing is to be performed the system would not need to undergo the tuning process. As more materials and geometries are tuned and tested, eventually the database can be expanded to a point where the tuning process may no longer be required to test any of the previously evaluated combinations. However, until there is sufficient documented operating parameters the tuning process is critical to optimal operation of the system.

The tuning process can also be performed manually. In both the automatic and manual tuning methods, the operating parameters are set before the test is run. In the automatic case the system will actuate the heating and cooling components when the specimen temperature reaches the maximum and minimum temperature bounds without additional user control. During manual tuning the system is set to the operating parameters and the heating element is turned on. The user must then monitor the specimen temperature and manually actuate the heater off and the cooler on when maximum temperature is observed. These two methods will both yield the same temperature profile data for tuning purposes and either is acceptable to prepare the system for phase two.

4.1.2 Phase 1 Discoveries

To begin testing, the thermocouples, cooling nozzles, and induction coil were placed in the same arrangement as expected for a final TMF test: as shown in Figure 4.2.

The major discovery as a result of the tuning experimentation was that the thermocouples selected were severely affected by the induction field. The sensors correctly read the specimen temperature at various points during test initialization while the induction heater was switched off. However, as soon as the heater was enabled the thermocouples would both display highly inaccurate temperature values: anywhere in the range of -1000°F to 1000°F. Immediately as the induction heater was deactivated, the thermocouples would return to reading correctly. During the design phase there was a concern with the induction field inducing a voltage in the thermocouple wires and altering the readouts. After speaking with the thermocouple supplier on possible preventative measures in the thermocouple selection/design, the recommendation was given to use the selected thermocouples featuring a ceramic sheath for the wires. This attempt to mitigate induction field effects appeared to be unsuccessful due to the previously mentioned incorrect readings, and Figure 4.3 illustrates the average

Figure IV.2: Tuning Test Arrangement

readings between the two thermocouples with the induction heater both off and on at 0.1 kW operating power and 650 kHz operating frequency.

An additional experiment was performed to determine the effective range of the induction field on system components. A single thermocouple was moved away from the induction coil in increments of one inch, when at each increment the induction heater was engaged and the thermocouple readings were observed. Through observing the readings, it was determined that at a distance of 8 inches from the coil the thermocouple was still affected by the induction field resulting in erroneous readings.

verify thermocouple wiring?

To continue with the tuning phase and acquisition of temperature values to determine heating and cooling rates, the pyrometer was used to monitor and log tem-

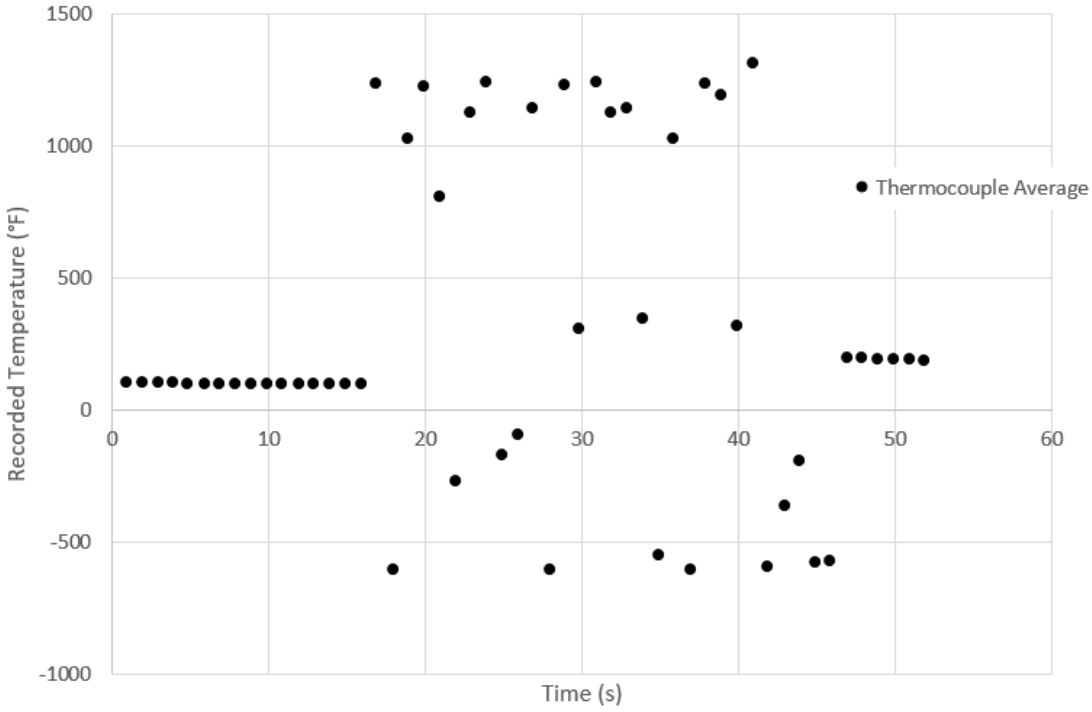

Figure IV.3: Thermocouple Operability

perature values with the previously mention emissivity calibration curve. Manual tuning needed to be performed due to the pyrometer being unable to integrate with the control system. The following sections outline the observed heating and cooling results from phase one manual testing.

4.1.3 Heating Results

Figure 4.4 displays the heating cycle results at the three selected operating powers of 1kW, 2kW, and 2.8kW. The results reflect expected trends with a lower operating heating power resulting in slower heating times. Additionally, the 1kW operating power is observed to be significantly more non-linear which is likely due to the radiant and convective losses increasing with specimen temperature. As the losses from ambient conditions grow at higher temperatures the heat input to the specimen is not great enough to maintain linear heating over the entire intended temperature range. Heating rate are estimated with a linear regression approximation for comparison with

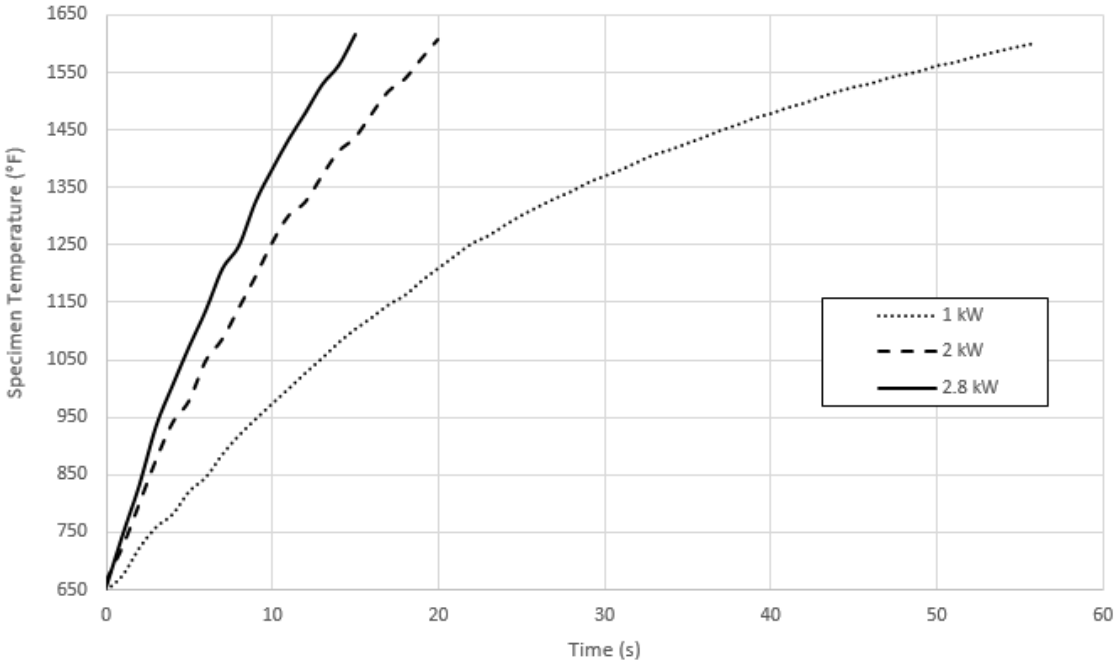

Figure IV.4: Phase 1 Heating Results at Three Operating Powers

commercial system cycle times as a baseline. From Figure 4.4 the shortest possible heating period time is determined to be 15 seconds at the 2.8kW operating power. It should also be noted that the recorded values are surface temperatures and may not accurately reflect the temperature at the radial center of the specimen. This presents a major challenge with testing solid specimens. The skin depth can be minimized by reducing operating frequency, but there is no way to verify the temperature at the radial center of the specimen during a test. Therefore, the shortest cycle time is also considered the optimal cycle time with the operating assumption that the radial temperature gradient is within an acceptable tolerance. Alternatively, longer cycle times may allow for more even heating through the center of the specimen and therefore may be instead considered optimal through future investigation. The heating results primarily portray the ability of the system to function and acquire informative data for the second phase.

Figure IV.5: Specimen Axial Temperature Gradient

Figure 4.5 depicts the specimen as observed by the operator during the heating portion of phase one experimentation. An observation from the heating tests is the color of the specimen while above 1000°F is not uniform over the gauge section. The ASTM standards require a temperature gradient of less than one percent over the gauge section, which is prominently not satisfied in the current configuration. A plausible solution to this issue is to acquire a coil with multiple turns that can evenly heat the entire gauge section and reduce the gradient to an acceptable level.

4.1.4 Cooling Results

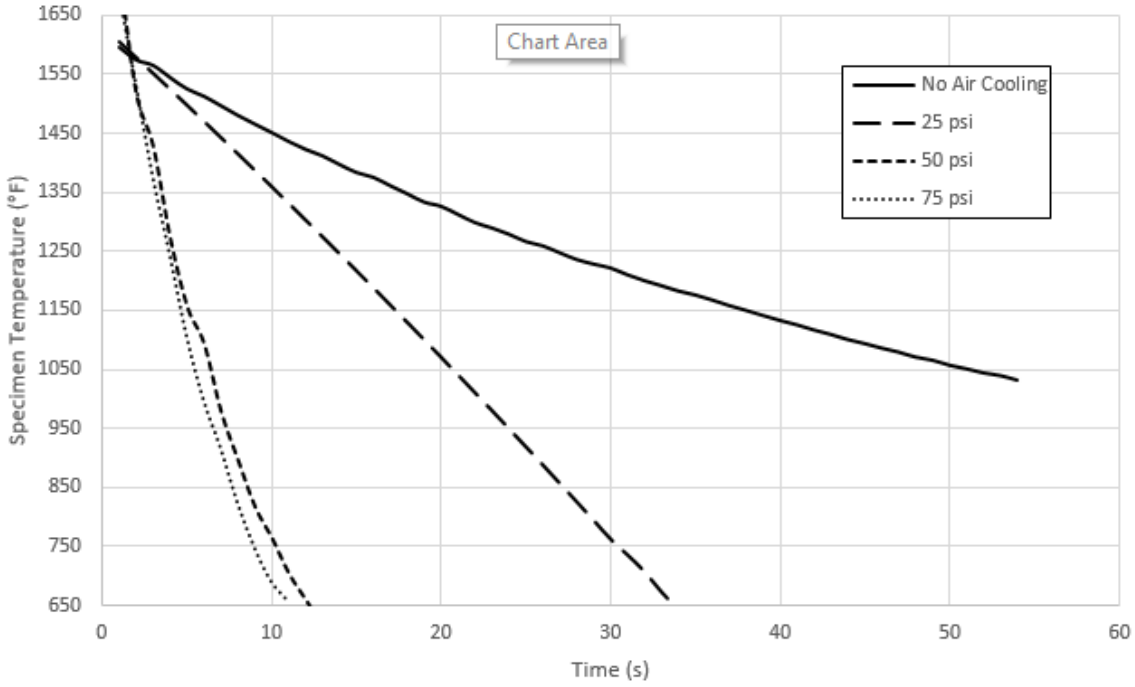

Figure IV.6: Phase 1 Cooling Results at Three Tool Pressures

Figure 4.6 displays the recording temperatures during the cooling period at the three selected operating compressor tool pressures. This data also includes a reference test performed with no cooling flow over the specimen. This baseline data has an estimate average cooling rate of 10°F/s, and does not traverse the intended temperature range in a reasonable period of time to consider for a TMF test. The cooling rates are determined in the same manner as the heating tests by utilizing a linear regression approach. As mentioned previously, the recorded temperatures are only for the surface and may not reflect the internal temperature of the specimen over the cooling range. Commercial solutions claim cooling rates of 9°F/s, and this is most likely an attempt to minimize the radial gradient during the cooling cycle. With this in mind, the fastest cooling times provided by the 75 psi and 50 psi operating pressures may not necessarily be the most ideal with the radial gradient in mind.

However, operating on the same assumption as the heating results, that the radial gradient is acceptable at all points in time, the 75 psi operating pressure provides the most efficient cooling time of approximately 10 seconds and cooling rate of 103 °F/s. The axial temperature gradient is assumed to also be improved as compared to the heating cycle due to the airflow being able to more evenly distribute over the gauge section whit favorable nozzle angles. Further work could also be performed to more thoroughly characterize the axial gradient and affected cooling rates at different nozzle angles.

4.1.5 Phase 1 Matrix and Results

Table IV.2: Resulting Tuning Test Matrix

Heater Power (kW)	**Heating Time (s)**	**Tool Pressure (psi)**	**Cooling Time (s)**
1	56	25	34
2	20	50	12
2.8	15	75	11

The resulting tuning test matrix displays the relationships developed between system operating parameters and the respective cycle times. This data is used to determine the cycle time as testing enters phase two. Cycles can be symmetric or asymmetric depending on the resulting times and dynamic loading machine capabilities. If a symmetric loading profile is desired, one functional cycle time can be determined as 40 seconds: with the induction heater operating at 2kW to heat in 20 seconds, and interpolating between 25 and 50 psi cooling times gives an operating compressor pressure of 41 psi to cool the specimen in 20 seconds. Alternatively, an asymmetric cycle time may consist of the induction heater operating at 2.8kW to heat the specimen in 15 seconds, and the compressor operating at 75 psi to heat the

specimen in 11 seconds, resulting in a total cycle time of 26 seconds. Additionally instead of interpolating to obtain exact heating and cooling times, the matrix resolution can also be further increased to obtain more accurate heating and cooling times, or the heating and cooling components can be fine-tuned to provide a predetermined desired cycle time.

4.2 Phase 2 - Profile Synchronization

The synchronization of the two loading profiles is another characteristic for validating system performance. Without thermocouple operation to allow for the control system to automatically regulate and synchronize the profiles, synchronization results could not be obtained. This section outlines the metrics developed to define and control profile synchronization along with example data to illustrate what well-synchronized and poorly-synchronized data may look like, as well as the methods developed to improve the synchronization to an acceptable level based on system response.

Two metrics will be used to evaluate the degree of profile synchronization: the point percent difference at each time step- referred to as Load Variance (L.V.), and the total accumulated time the loading profiles are outside of the acceptable tolerance-denoted by Accumulated Load Variance (A.L.V.). To calculate each of these parameters, the profiles must first be characterized in a non-dimensional way at any specific time-step within the cycle. Non-dimensional characterization of the loading profiles is achieved by equations 4.2.1 and 4.2.2 below. The two parameters describe the temperature and strain at any given time as a percent of the defined maximum value for each measurement.

$$T_{load} = \frac{T_i - T_{min}}{T_{max} - T_{min}} * 100 \tag{4.2.1}$$

Equation 4.1 describes the thermal profile loading as a percentage, where T_i is instantaneous temperature, T_{max} is maximum temperature, and T_{min} is minimum

temperature, all of which measured in Fahrenheit.

$$M_{load} = \frac{\varepsilon_i - \varepsilon_{min}}{\varepsilon_{max} - \varepsilon_{min}} * 100 \tag{4.2.2}$$

Equation 4.2 describes the strain profile loading as a percentage, where ε_i is instantaneous strain, ε_{max} is the maximum strain, and ε_{min} is the minimum strain.

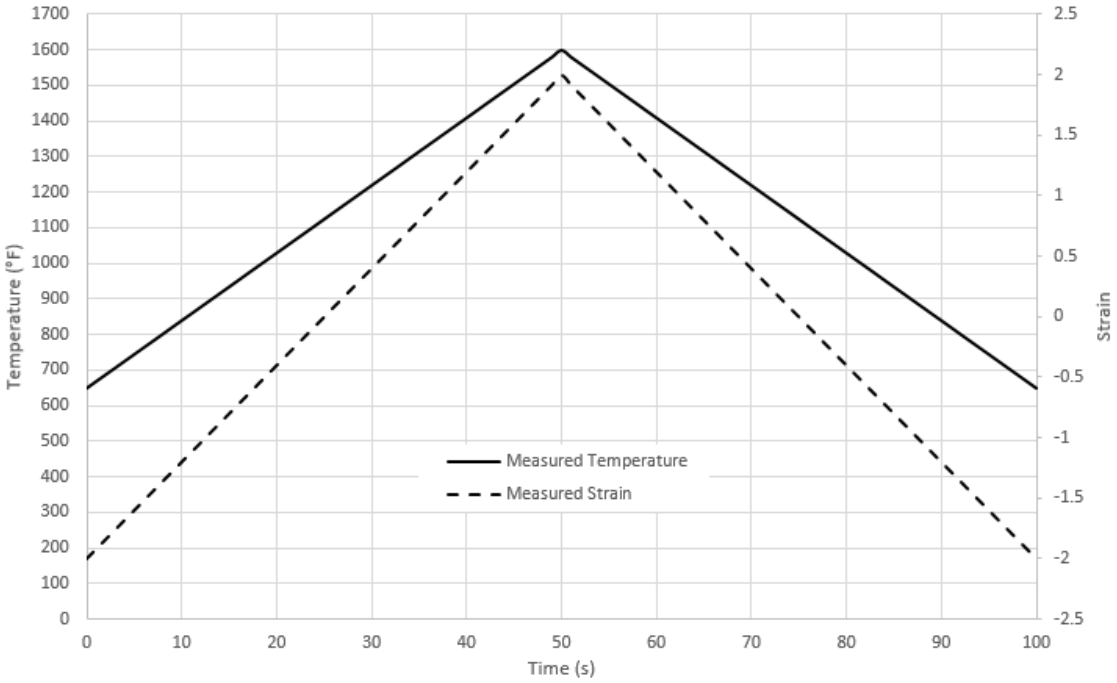

Figure IV.7: Example Of Raw Data From A Synchronized Cycle

Figure 4.7 and 4.8 further illustrate the use of the above two parameters. Figure 4.7 depicts the measured temperature and measured strain as perfectly synchronized profiles over a randomly selected cycle time of 100 seconds. From this chart it is not apparent the two profiles are perfectly synchronized and therefore would be difficult to develop metrics to determine if the profiles are synchronized or not from raw data alone. Figure 4.8 depicts the two loading profiles once the data is converted to normalized values using the M_{load} and T_{load} equations over the same cycle and loading ranges. Both profile reach a ratio of 100% in the same instant at 50 seconds and it is

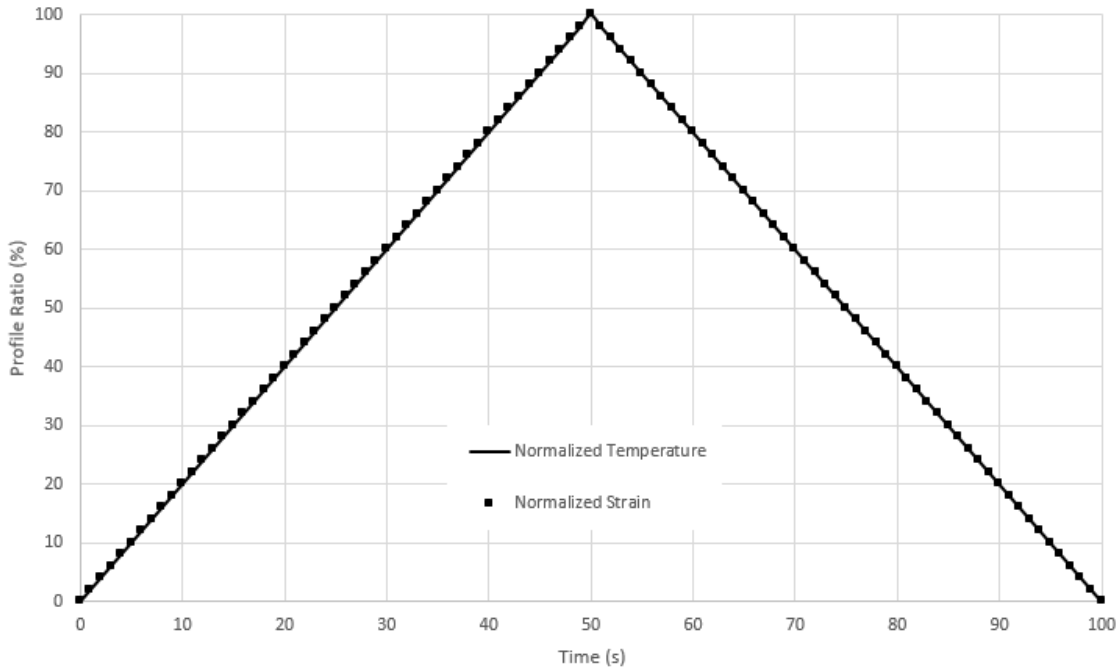

Figure IV.8: Example Of Normalized Data From A Synchronized Cycle

much more clear that the two profiles are synchronized throughout the course of the test.

With the non-dimensional loading parameters characterized, the Load Variance and Accumulated Load Variance can be calculated with Equations 4.2.3 and 4.2.4 below.

$$L.V. = |M_{load} - T_{load}| / \frac{M_{load} + T_{load}}{2} \tag{4.2.3}$$

In realistic data the thermal loading profile will not be perfectly aligned as previously shown as the temperature will fluctuate slightly relative to the mechanical loading profile as the induction heater actuates on and off to maintain synchronization. The load variance variable is introduced here, as a percent difference between the two loading parameters at any moment during the test, to define the bounds for the maximum allowable difference between the profiles throughout the entire cycle. Figure 4.9 illustrates these bounds on a portion of Figure 4.8 (between 20 and 35

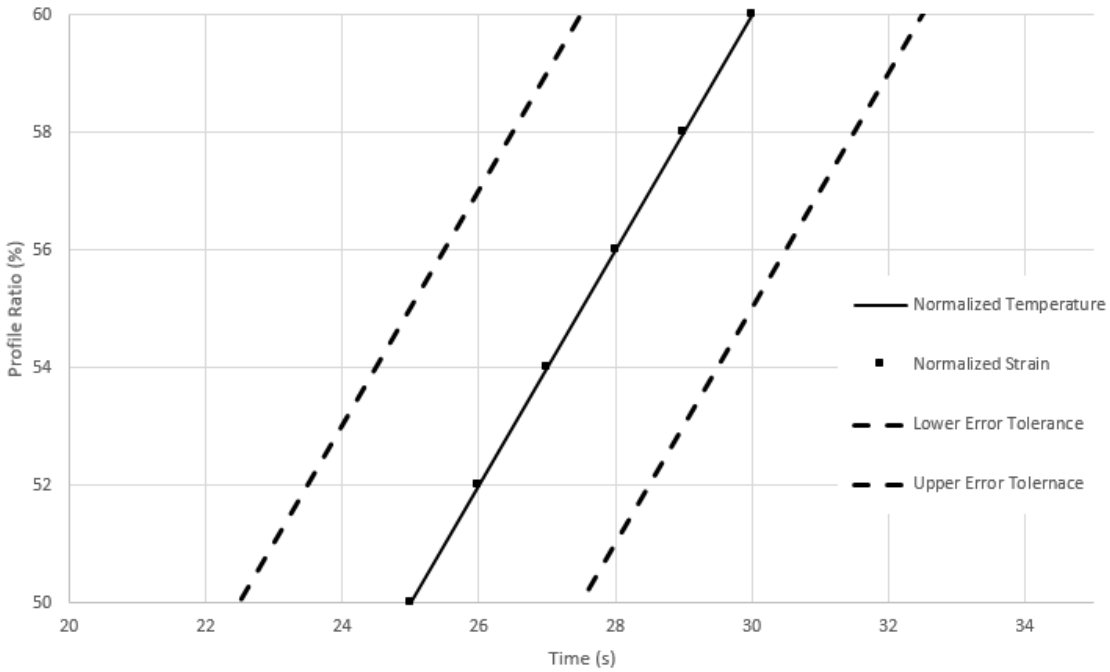

Figure IV.9: Load Variance Maximum Allowable Error

seconds, and between 50 and 60 percent) with the bounds set to ± 5% . Initially, the bounds are set as the control threshold serving as the values the control system uses to turn the heating system on or off (or cooling system if during the cooling period) to retain synchronization.

$$A.L.V. = \sum_{0}^{t=i} \frac{(\Delta t_i)_{L.V.}}{t_{cycle}} \tag{4.2.4}$$

Where $(\Delta t_i)_{L.V.}$ is the amount of time the two loading profiles are outside of the acceptable tolerance, and t_{cycle} is the total cycle time.

During acceptable system operation, the two profiles are considered to be well-synchronized as long as the thermal loading profile remains within the tolerance bounds. To characterize synchronization beyond good or bad, the accumulated load variance variable is introduced to define how well or how poorly the profiles align. Displayed in Figure 4.10 is an example of how the A.L.V. would be calculated for

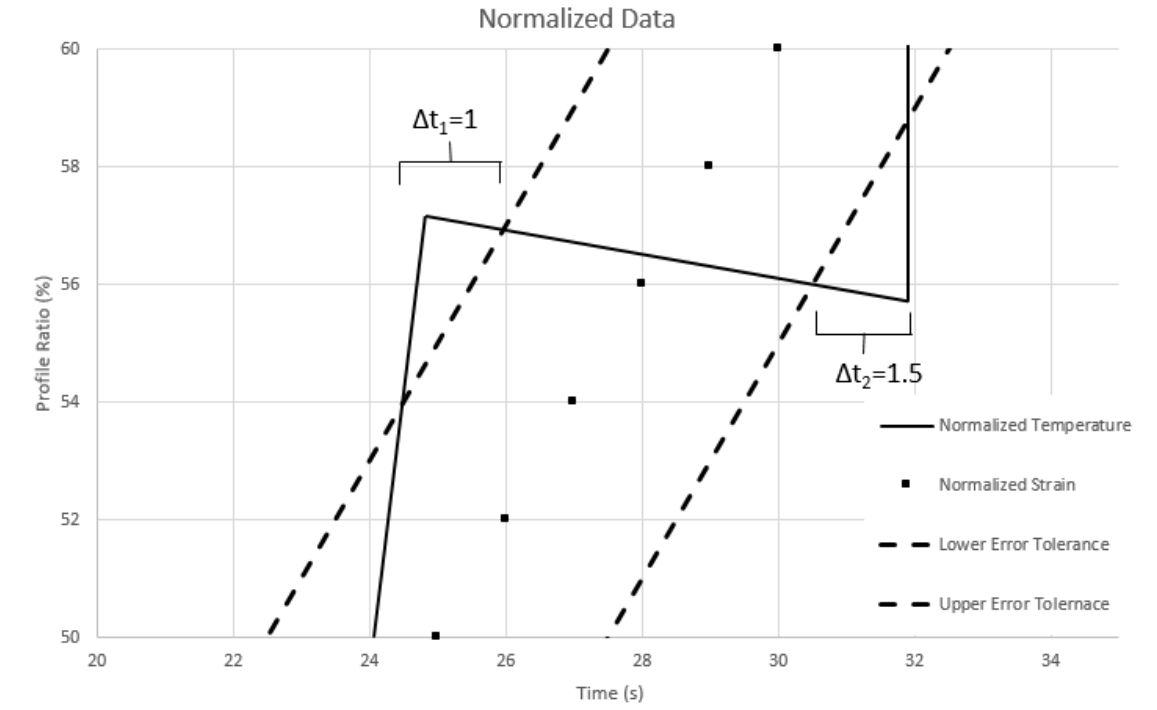

Figure IV.10: Example Accumulated Load Variance Calculation

a poorly synchronized profile over the same section of the cycle depicted in Figure 4.9. The accumulated load variance for the section depicted could be determined by summing the total time the profile is outside of the acceptable tolerance (Δt_1 and Δt_2) and dividing by the total cycle time (for the example section depicted in the figure, 5 seconds is used) to obtain a total A.L.V. value of 0.5, or alternatively the profile is outside of the allowable tolerance 50% of the time.

The path to achieving perfectly synchronized profiles is more clearly defined after developing the previous metrics: developing the system to obtain an A.L.V. value of zero. To achieve this level of synchronization, the control system must utilize more strict bounds to actuate the thermal loading systems. Figure 4.11 illustrates another set of example data where the system operates by actuating the heating or cooling components based on a control tolerance of ± 2.5% in order to keep the thermal loading profile within the actual allowable tolerance of ± 5%. The actual allowable load variance tolerances must be determined by the user based on the test

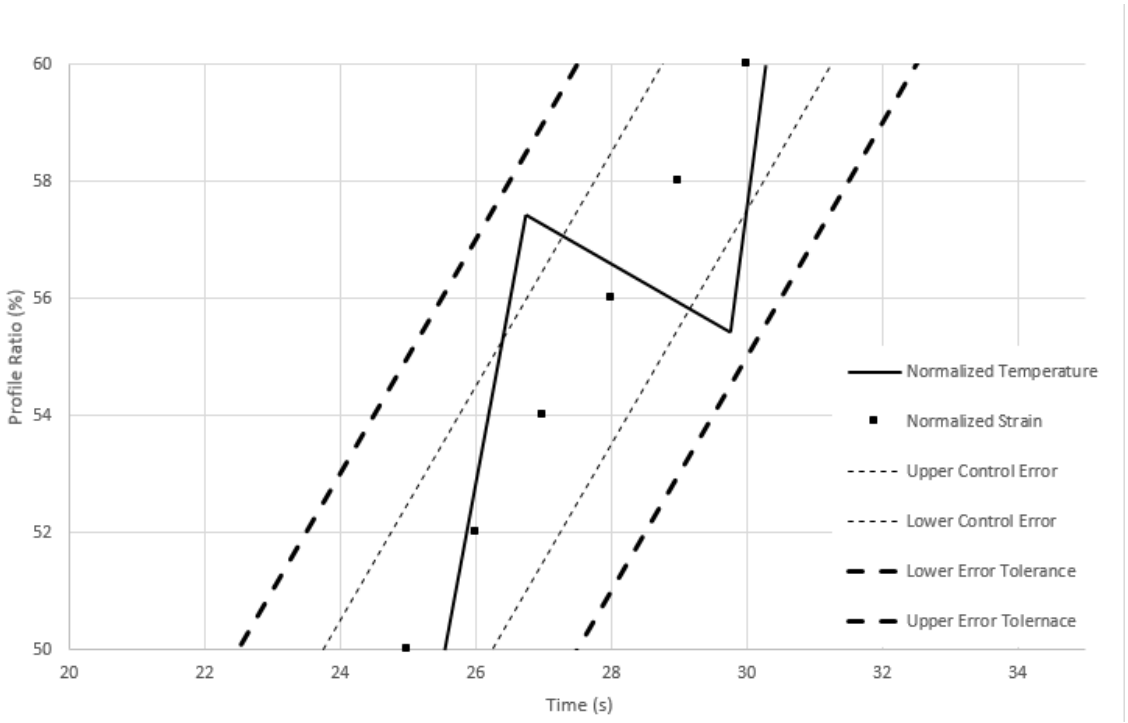

Figure IV.11: Example Profile Synchronization with Improved Control Bounds

intended to be performed, but the control load variance tolerances must be determined experimentally during the second phase. This is the primary objective of the second phase as the necessary control tolerances to account for varying temperature system response rates may vary with many factors such as specimen material geometry, coil geometry, operating frequency, operating power, operating tool pressure, nozzle alignment, and ambient conditions.

4.2.1 TMF Test Control Logic

Figure 4.12 illustrates an overview of the code operation with a flow chart for ease of understanding. The basic functions are outlined, but there are some details such as latch variables to hold the control scheme into either the cooling or heating control and the specifics on the initialization and dwell functions. These functions are specific to the sensor wiring and dynamic test machine control setup and are displayed in Appendix C.

The control system operates by firstly constantly monitoring if the specimen is broken through a procedure that performs a check if the strain is unchanged after a certain period of time (also a routine specific to the dynamic load machine operation). As long as the specimen is not broken, the strain at the previous and current time step are compared to establish whether the slope of the mechanical loading profile is positive or negative to determine if the system is in the heating or cooling cycle. If the slope value is returned as zero, a check is performed to compare the measured strain with the previously defined maximum and minimum strain values. If the observed strain is greater than the maximum or less than the minimum, the system will update the relative strain bound with the observed value. This process accounts for redefining the strain bounds at every local maximum or minimum to account for creep over the course of the thousands of cycles. When the slope is returned as a non-zero and the appropriate cycle type is identified based on a latch variable, the routine then calculates the current load variance and determines if it is within the control load variance that was set by the user. If the load variance is within tolerance the system prints the strain and temperature values to the serial monitor and after a 0.5 second delay repeats the loop. If the load variance is determined to be outside of the control tolerance the system will then actuate the cooling on or off in the cooling period, or the heater on or off in the heating period, based on whether the thermal load is too high or too low. Once actuated, the system then returns to the previously mentioned serial print and delay function before repeating the loop. If at any point during the test the specimen is determined to be broken, the system will disable all components and end the test.

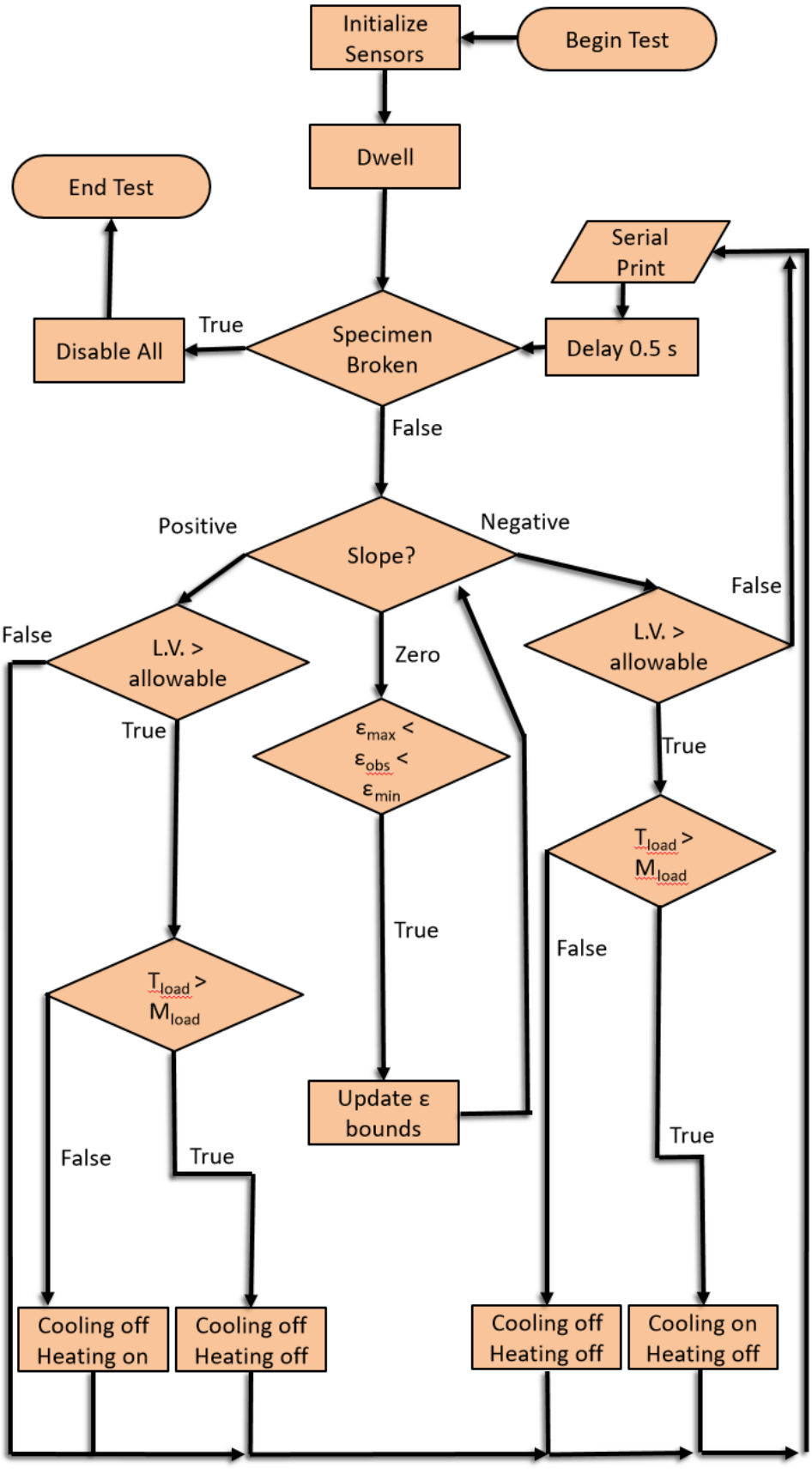

Figure IV.12: TMF Test Control Flow Chart

CHAPTER V

Conclusions

The system design illustrates successful integration and operation of many components vital to performing TMF testing. All components that were designed to interface with and be operated by the controller were able to do so, and the same components were able to acquire informative data about the heating and cooling performance of the system. One major observation during the experimental phase was the difficulty of operating components near an induction field. Using induction for the method of heating was found to perform as well as expected for directly heating a specimen quickly without the need for a large furnace or container. However, the additional complexity of operating thermocouples within the induction field was not solved within the course of this study.

The system was determined to be able to achieve heating times of as low as 15 seconds, and cooling times as low as 11 seconds in the desired temperature range of 650°F to 1600°F. The heating of the INC718 specimen within these time periods exactly matches the initial heating period estimate of 15 seconds, and the cooling time greatly outperforms the initial cooling period estimate of 45 seconds. However, both components cannot guarantee a minimal radial temperature gradient at the current cycle times, and presents the main difficulty with testing a solid specimen. The ASTM E2368 recommendation to utilize a hollow tubular specimen is for reducing the concern about a gradient within the specimen. With the current induction heater, the skin depth penetration cannot be increased to reach the center of the specimen

by increasing frequency. Additionally, with the solid specimen the cooling flow can only pass over the outer surface of the specimen resulting in an unfavorable radial gradient. Alternatively, the use of a tubular specimen may allow the cooling system to also direct flow through the center of the specimen to guarantee there is no notable gradient between the inner and outer surfaces.

5.1 Implications for Practice

This experimental apparatus delivers the ability to perform TMF testing on a variety of universal test machines due to the high versatility and low independent part cost of the system. Usability may vary by the intended test material and specimen geometry, but the majority of common materials and geometries are compatible with the final design. Temperature can be monitored and maintained within a tolerance of the mechanical loading determined by the test administrator. The accuracy of synchronization must also be determined by the user depending on the requirements necessary for the each specific test.

The system requires a high level of user interaction and preparation before any test can be performed. This level of user involvement does raise the difficulty to a point that the user must be familiar with all system components, as well as have access to a high temperature furnace with the knowledge to perform the pyrometer emissivity calibration process. The system also can be operated without the pyrometer for temperature validation at the center of the specimen due to the pyrometer not being necessary in the operational processes, but will lack valuable post-test information on the specimen status throughout the test.

Once the operator or organization has completed testing with a certain material and geometry, all calibration and operational conditions (such as operating frequency, power, cycle times, etc.) should be documented. In addition, before each test the tuning and profile synchronization testing should be performed to determine optimal

cycle times and control tolerance bounds. Documenting all of the operational values will reduce future testing times, so long as the geometry and material fabrication processes are unchanged. As more materials are tested, the user can build up a database of operating settings specific to their machine and set-up. The databases may also be later compared with databases accumulated by other users to reference and compare the operating conditions and TMF test results for validation and improvement of test conditions.

5.2 Limitations

The main limitations listed below exclude obvious bounds such as the maximum temperature, minimum heating/cooling time, and other limitations that are set by component-ratings. The following discussion primarily includes limitations set by the system design, and not by component operability range.

One of the major, and most prominent, limitations of the system is the requirement of the test material to be ferromagnetic. While this does allow for testing of many common aerospace materials, there are many that cannot be evaluated thermomechanically with this apparatus. This limitation does serve a benefit to the design of the system or the addition of new sensors by allowing any part not intended to be heated near the coil to be made out of a non-ferromagnetic material. This ability further expands the versatility and modifiability of the system.

Another limitation of the system is the difficulty with performing alternate phase-synchronization testing. To perform a test with out-of-phase synchronization, the control code would need to be moderately modified, and the synchronization metrics such as load variance and accumulated load variance would also need to be modified within the control code to account for the new phase requirements. Once a new control sequence has been created for out-of-phase testing, applying that code to an existing system would take minimal time and effort. Creating the out-of-phase code

sequence was not a priority in the scope of the current project.

5.3 Recommendations

This design operates within the intended design expectations, however there are several major improvements that could be made to improve the profile synchronization accuracy as well as other parameters to benefit the overall system design. Firstly, the implementation of an improved induction heater could have major effects on the temperature profile control. An improved induction heater would have the ability to digitally actuate the input power to manipulate the rate of heating during a test. This extra level of control would allow for the control system to recognize how high the load variance is and automatically adjust the heating rate, through changing the heater power level, to more accurately synchronize with the mechanical profile during the heating phase of the cycle. This improved heater should also have a higher output operating power to increase the linear heating range and overall heating rates if a shorter cycle time is desired.

The same improved level of control as mentioned previously could be achieved in the cooling cycle by implementing a solenoid with the ability to actuate the flow rate or tool pressure. It is also recommended that this solenoid be rated at a pressure greater than, or equal to, the maximum available pressure of the connected air compressor. Just as with the improved induction heater, this would allow for active adjustment of the air flow rate during a cycle to more accurately match the cooling profile of the specimen with the mechanical loading profile.

Improving the coil design is determined as a necessary improvement to the system in order to minimize the axial temperature gradient. As mentioned previously, the current coil design results in a non-uniform axial temperature distribution that is greater than the allowable tolerance set by ASTM E2368. To correct this, a multi-turn coil should be implemented. The coil should have the same axial length as the gauge

section and include enough space between the coils to accommodate for pyrometer measurements and extensometer connections to the specimen. This would not only improve heating uniformity, but also the heating rates and control by allowing for a larger concentration of current to be directed into the specimen. This expanded heating profile may also prove to increase the heating of the grips, and for that reason it may also be recommended in turn to implement a grip style with water cooling adaptability on the desired dynamic test machine.

The final recommendation for improvement and completion of the system is to acquire thermocouples with adequate shielding to operate within an induction field. Some element of the design could incorporate a shield of ferromagnetic material around the entirety of the thermocouple with a thickness greater than the penetration depth of the induction field. This would provide adequate shielding of the sensors without interfering with temperature measurement. Alternatively, if a hollow specimen is tested, the sensors could instead be placed within the specimen to monitor temperature from the inner surface. The specimen wall thickness would need to be large enough to ensure the induction field does not penetrate to the internal sensors, but still small enough to allow for adequate radial temperature distribution. Either method should provide adequate shielding to protect the specimen from inductive interference and result in the intended operation of the system.

REFERENCES

[1] *Standard Practice for Strain Controlled Thermomechanical Fatigue Testing*, Standard, American Society for Testing and Materials, December 2004.

[2] K. Bhanu Sankara Rao and B. Raj, *Fatigue testing: Thermal and thermomechanical*, Encyclopedia of Materials: Science and Technology (K.H. Jürgen Buschow, Robert W. Cahn, Merton C. Flemings, Bernhard Ilschner, Edward J. Kramer, Subhash Mahajan, and Patrick Veyssière, eds.), Elsevier, Oxford, 2001, pp. 2999–3001.

[3] T. Brendel, E. Affeldt, J. Hammer, and C. Rummel, *Temperature gradients in tmf specimens. measurement and influence on tmf life*, International Journal of Fatigue **30** (2008), no. 2, 234–240, High Temperature Thermo-mechanical Fatigue: Testing Methodology, Interpretation of Data, and Applications.

[4] Encyclopedia Britannica, *Pyrometer*, Available at https://www.britannica.com/technology/pyrometer.

[5] Tomasz Bury, *Impact of a medium flow maldistribution on a cross-flow heat exchanger performance*, Heat Exchangers (Jovan Mitrovic, ed.), IntechOpen, Rijeka, 2012.

[6] J. Codrington, P. Nguyen, S.Y. Ho, and A. Kotousov, *Induction heating apparatus for high temperature testing of thermo-mechanical properties*, Applied Thermal Engineering **29** (2009), no. 14, 2783–2789.

[7] Wenkai Deng, Jinghao Xu, Yunming Hu, Zaiwang Huang, and Liang Jiang, *Isothermal and thermomechanical fatigue behavior of inconel 718 superalloy*, Materials Science and Engineering: A **742** (2019), 813–819.

[8] G.A Greene, C.C Finfrock, and T.F Irvine, *Total hemispherical emissivity of oxidized inconel 718 in the temperature range 300–1000°c*, Experimental Thermal and Fluid Science **22** (2000), no. 3, 145–153.

[9] Matej Kranjec, Jernej Korinšek, Miha Ambrož, and Robert Kunc, *Control system for a tensile-testing device using low-cost hardware and open-source software*, Strojniški vestnik - Journal of Mechanical Engineering **66** (2020), no. 3, 155–163.

[10] V. MAUREL, A. KOSTER, and L. RÉMY, *An analysis of thermal gradient impact in thermal–mechanical fatigue testing*, Fatigue & Fracture of Engineering Materials & Structures **33** (2010), no. 8, 473–489.

[11] C J MORRISON, *10 - high frequency heating methods for materials testing at ultra high temperatures*, Ultra High Temperature Mechanical Testing (R D LOHR and M STEEN, eds.), Woodhead Publishing, 1995, pp. 128–147.

[12] Norman S. Nise.

[13] J. Palmer, J. Jones, A. Dyer, R. Smith, R. Lancaster, and M. Whittaker, *Development of test facilities for thermo-mechanical fatigue testing*, International Journal of Fatigue **121** (2019), 208–218.

[14] Mayur Patil, Rahul Kumar Choubey, and Prashant Kumar Jain, *Influence of coil shapes on temperature distribution in induction heating process*, Materials Today: Proceedings **72** (2023), 3029–3035, 2nd International Conference on Sustainable Materials, Manufacturing and Renewable Technologies 2022.

[15] Lihe Qian, Z. Wang, Hiroyuki Toda, and Toshiro Kobayashi, *Effect of reinforcement volume fraction on the thermo-mechanical fatigue behavior of sic w/6061al composites*, Materials Science and Engineering A-structural Materials Properties Microstructure and Processing - MATER SCI ENG A-STRUCT MATER **357** (2003), 240–247.

[16] Przylucki R. Smalcerz, A., *Impact of electromagnetic field upon temperature measurement of induction heated charges*, International Journal of Thermophysics **34** (2013), 667–669.

[17] Wen Sun, Ayan Bhowmik, Adrian Wei-Yee Tan, Ruitao Li, Fei Xue, Iulian Marinescu, and Erjia Liu, *Improving microstructural and mechanical characteristics of cold-sprayed inconel 718 deposits via local induction heat treatment*, Journal of Alloys and Compounds **797** (2019), 1268–1279.

[18] MTS Systems, *Dynamic material test systems*, Available at https://www.mts.com/en/products/materials/dynamic-materials-test-systems/landmark-servohydraulic.

[19] Henrik Zaletelj, Gorazd Fajdiga, and Marko Nagode, *Numerical methods for tmf cycle modeling*, Strojniški vestnik-Journal of Mechanical Engineering **57** (2011), no. 6, 485–494.

APPENDIX A

Bill Of Materials

Supplier Name	Part #	Description	Quantity	Cost/Unit, Excluding Shipping
Arduino CC	A000066	Arduino Uno REV3, blue-green color	1	$30.16
Arduino CC	A000110	Arduino 4 Relays Shield, blue-green color with white relays	1	$30.16
Adafruit	269	Thermocouple Amplifier with 2 terminal	2	$14.95
McMaster-Carr	47065T101	80/20, 1"x1", 5 ft solid	7	$29.23
McMaster-Carr	3136N159	Flush Tee 1" Rail Surface Bracket for Single Rails	1	$17.88
McMaster-Carr	47065T101	80/20, 1"x1", 2 ft solid	2	$12.17
McMaster-Carr	47065T267	90 Degree Angle Surface Bracket for Single Rails	5	$11.60
McMaster-Carr	47065T236	1" Corner Bracket Single Rail Silver	8	$7.92
Zoro	G304393775	Rubber Hose Whip w/o chuck 12 Inch	3	$10.35
Omega	OS801A-USB	Modbus IR Transmitter with 4-20 mA and USB outputs, close focus, 2.2 microns	1	$578
Omega	OSUSB-ABL	Adjustable bracket for IR-USB	1	$44.76
U.S. SOLID	USS2-00051	1/4" NPT Brass Electric Solenoid Valve 12VDC Normally Closed	1	$18.99
SmoTecQ	B077PW5JC3	12V 2A Power Supply AC Adapter, AC 100-240V to DC 12 Volt Transformers	1	$12.99
Taisher	B086DGR3CJ	Brass 3-Way Hex Style Air Manifold	1	$18.99
Across International	Wac-1	Chiller	1	$2,993
Epsilon	Epsilon 3448	High Temperature Self Supporting Furnace Extensometer	1	$3,738
McMaster-Carr	3860K204	Thermocouple Probe for Solids, Type K, 2.5 Second Response	2	$25.66
McMaster-Carr	47065T205	Rail to Tube for Single Rails	2	$50.33
McMaster-Carr	5537T352	Sensor Holder	2	$4.23
McMaster-Carr	47065T893	Gusset Bracket, 2" Long 2" High Double/Quad Rail Framing	5	$25.63
McMaster-Carr	47065T236	Silver Corner Bracket, 1" Long for 1" High Rail Framing	16	$7.92
McMaster-Carr	47065T267	T-slot Framing, Silver Corner Surface Bracket for 1" High Single Rail	4	$11.60
McMaster-Carr	47065T107	Solid Double 6 Slot, 10 ft	2	$79.76
Amazon		Amazon Basics USB 2.0 Extension Cable - A-Male to A-Female Adapter Cord 3 meters	1	$5.23
Amazon		Parkworld 886382 Adapter Cord NEMA 14-30P Male to L6-20R Female, 20A, 250V, 1.5FT	1	$39.99
Amazon		KSACE 12V 2A Power Supply Adapter, AC100-240V to DC 12V Transformers	1	$8.88
Amazon		Interstate Pneumatics Tw100 Rubber Hose Whip Without Chuck 12 in Long	1	$12.24
Amazon		Taisher 3-Way 1/4 in NPT Hex Style Air Manifold with 3 Pieces Brass Industrial Coupler and Plug	1	$19.19

Lowe's	877189	1/4in MIP Square Head PL	1	$3.88
Lowe's	877073	1/2in BARB X MIP Adaptor	2	$6.38
Lowe's	20116	1/2in Black Iron Plug	2	$2.08
Lowe's	877250	1/4in MIP X 6in Pipe NI	1	$12.48
Lowe's	814318	20 ft PVC Tubing 3/8in	1	$11.40
Lowe's	456833	Pipe Tape 1/2in	1	$2.58
Lowe's	879265	1/2in Clear Vinyl 20-	1	$11.49
Lowe's	31448	RBR Purchasing 6in X 6in X 1/8in	2	$2.70
Lowe's	877082	3/8in BARB to 1/4in BARB	2	$3.98
Lowe's		Water Pump + Trash Bin		$143.48
Rosin Power	IGH06A3	6.6 kW Induction Heater	1	$ 5,930.10
Across International	N/A	Custom Induction Coil *1.25" diameter, 1-turn)	1	$ 180.00

APPENDIX B

Tuning Control Code

TMF_Tuning_Data_Control_Logic.ino

```
#include <SPI.h>
#include "Adafruit_MAX31855.h"

// Thermocouple software SPI digital pins
#define MAXDO1   2
#define MAXCS1   3
#define MAXCLK1  5

#define MAXDO2   9
#define MAXCS2   10
#define MAXCLK2  11

// initialize the Thermocouples
Adafruit_MAX31855 thermocouple1(MAXCLK1, MAXCS1, MAXDO1);

Adafruit_MAX31855 thermocouple2(MAXCLK2, MAXCS2, MAXDO2);

// initialize the relays
int relay_1 = 4;

int DataPosPin = A3; // Extensometer Pos connected to analog pin 3 outside leads to ground and +5V
int DataNegPin = A4; // Extensometer Neg connected to analog pin 4 outside leads to ground and +5V
int val1 = 0;  // variable to store the value read
int val2 = 0;  // variable to store the value read


double MinTemp = 650;
double MaxTemp = 1598;
double thermo1 = thermocouple1.readFahrenheit();
double thermo2 = thermocouple2.readFahrenheit();
double thermoavg = (thermo1 + thermo2)/2;

void setup() {
  Serial.begin(9600); //BAUD Rate 9600

  pinMode(relay_1, OUTPUT);
  digitalWrite(relay_1, LOW);
  // pinMode(relay_2, OUTPUT);

  Serial.println("Relays Initialized");

  while (!Serial) delay(1); // wait for Serial on Leonardo/Zero, etc

  Serial.println("MAX31855 test");
  // wait for MAX chip to stabilize
```

```
  delay(500);
  Serial.print("Initializing sensor...");
  if (!thermocouple1.begin()) {
    Serial.println("ERROR.");
    while (1) delay(10);
  }

    if (!thermocouple2.begin()) {
    Serial.println("ERROR.");
    while (1) delay(10);
  }

  double thermo1 = thermocouple1.readFahrenheit();
  double thermo2 = thermocouple2.readFahrenheit();
  double thermoavg = (thermo1 + thermo2)/2;

  Serial.println("DONE.");


  return;
}

int main(){

  setup();
  logging1();
  logging2();
  return 0;
}




void logging1(){
  //heater on
  //air off
  if (thermoavg < MaxTemp){

    delay(1000); //delay between measurements

    thermo1 = thermocouple1.readFahrenheit();
    thermo2 = thermocouple2.readFahrenheit();
    thermoavg = (thermo1 + thermo2)/2;

    Serial.print(thermo1);
```

```
    Serial.print(",");
    Serial.print(thermo2);
    Serial.print(",");
    Serial.print(thermoavg);
    Serial.println();
  }
  else if (thermoavg >= MaxTemp){
    return;
  }
}

void logging2(){
  //heater off
  //air on
  if (thermoavg > MinTemp){

    delay(1000); //delay between measurements

    thermo1 = thermocouple1.readFahrenheit();
    thermo2 = thermocouple2.readFahrenheit();
    thermoavg = (thermo1 + thermo2)/2;

    Serial.print(thermo1);
    Serial.print(",");
    Serial.print(thermo2);
    Serial.print(",");
    Serial.print(thermoavg);
    Serial.println();
  }
  else if (thermoavg <= MinTemp){
    //air off
    return;
  }
}
```

APPENDIX C

Main Control Code

TMF_Main_Control_Logic_thermocouples.ino

```
#include <SPI.h>
#include "Adafruit_MAX31855.h"

// Thermocouple software SPI digital pins
#define MAXDO1   2
#define MAXCS1   3
#define MAXCLK1  5

#define MAXDO2   9
#define MAXCS2   10
#define MAXCLK2  11

// initialize the Thermocouples
Adafruit_MAX31855 thermocouple1(MAXCLK1, MAXCS1, MAXDO1);

Adafruit_MAX31855 thermocouple2(MAXCLK2, MAXCS2, MAXDO2);

// initialize the relays
int relay_1 = 4;

int DataPosPin = A3; // Extensometer Pos connected to analog pin 3 outside leads to ground and +5V
int DataNegPin = A4; // Extensometer Neg connected to analog pin 4 outside leads to ground and +5V
int val1 = 0;  // variable to store the value read
int val2 = 0;  // variable to store the value read

void setup() {
  Serial.begin(9600); //BAUD Rate 9600

  pinMode(relay_1, OUTPUT);
  digitalWrite(relay_1, LOW);
  // pinMode(relay_2, OUTPUT);

  Serial.println("Relays Initialized");

  while (!Serial) delay(1); // wait for Serial on Leonardo/Zero, etc

  Serial.println("MAX31855 test");
  // wait for MAX chip to stabilize
  delay(500);
  Serial.print("Initializing sensor...");
  if (!thermocouple1.begin()) {
    Serial.println("ERROR.");
    while (1) delay(10);
  }

    if (!thermocouple2.begin()) {
    Serial.println("ERROR.");
```

```
    while (1) delay(10);
  }

  Serial.println("DONE.");

  extpos = analogRead(DataPosPin);  // read the Pos pin
  extneg = 1023 - (analogRead(DataNegPin);  // read the Neg pin
  ext = extpos - extneg //extensometer delta
  extzero = abs(ext)<=10
  if (extzero == true) { //check that extensometer readings are zeroed +-5 Analog Units from 512
    Serial.println("Extensometer Ready")
  }
  else {
  Serial.println("Extensometer Not Zeroed")
  }

  double thermo1 = thermocouple1.readFarenheit();
  double thermo2 = thermocouple2.readFarenheit();
  thermoavg = (thermo1 + thermo2)/2

  return ext, thermoavg, extzero
}

//Initializing and Declaring Values
int MinTemp = 650; //F
int MaxTemp = 1598; //F
int TempRange = MaxTemp - MinTemp
int MinMech = -1000; //Digital Units
int MaxMech = 1000; //Digital Units
double thermo1 = thermocouple1.readFahrenheit(); //Declare First Thermocouple
double thermo2 = thermocouple2.readFahrenheit(); //Declare Second Thermocouple
double thermoavg = (thermo1 + thermo2)/2; //Declare Average Metric
double TRatio = ((themroavg-MinTemp) / TempRange )*100; //Temperature Loading Profile Tracking (as percent)
double MRatio = (ext-MinMech) / (MaxMech-MinMech)*100; // mechanical profile tracking (as percent)
int PD = 0.05; //Maximum Allowable Percent Difference between profiles (as a decimal)
bool SpecimenBroken = False;


double current = ext;
double previous = 0;

void main(){
  setup();
  slope(double);
  dwell();
  cycle(double, bool);
}
```

```
95
96  void slope(double ext){
97    previous = current;
98    current = ext;
99    slope = previous - current;
100   return slope;
101 }
102
103 void SpecimenBroken(){
104   Specimen Broken = False;
105   return;
106 }
107
108
109
110 void cycle(double ext, thermoavg, slope, bool extzero){
111   while (SpecimenBroken = false){
112     delay(500);
113     while (slope > 0 or ext = MinMech){
114       //turn heater on
115       //turn cooling off
116
117       if (abs((TRatio-MRatio)/((TRatio+MRatio)/2)) >= PD){
118         if (TRatio > MRatio){
119           //turn off heat
120         }
121
122         else if (TRatio < MRatio){
123           //turn on heat
124         }
125       }
126
127       if (ext > MaxMech){
128         MaxMech = ext;
129       }
130       else if (ext < MinMech){
131         MinMech = ext;
132       }
133       slope();
134     }
135     while (slope < 0 or ext = MaxMech){
136       //cooling on
137       //heating off
138       if (abs((TRatio-MRatio)/((TRatio+MRatio)/2)) >= PD){
139         if (TRatio > MRatio){
140           //turn on cooling
141         }
```

```
142             else if (TRatio < MRatio){
143               //turn off cooling
144             }
145           }
146
147           if (ext > MaxMech){
148             MaxMech = ext;
149           }
150           else if (ext < MinMech){
151             MinMech = ext;
152           }
153           slope();
154         }
155
156
157       }
158
159       while (specimen broken = true){
160         //turn off heat
161         //turn off air
162         return
163       }
164
165
166
167
168     }
169
```

VITA

Haden Glasgow

Candidate for the Degree of

Master of Science

Thesis: DESIGN AND VALIDATION OF A VERSATILE THERMOMECHANICAL FATIGUE TEST SYSTEM RETROFIT KIT

Major Field: Mechanical and Aerospace Engineering

Biographical:

Education:

Completed the requirements for the Master of Science in Mechanical and Aerospace Engineering at Oklahoma State University, Stillwater, Oklahoma in May, 2023.

Completed the requirements for the Bachelor of Science in Mechanical and Aerospace Engineering at Oklahoma State University, Stillwater, Oklahoma in May, 2021.

Experience:

Graduate Research Assistant - Oklahoma State University, Stillwater, OK
Graduate Teaching Assistant - Oklahoma State University, Stillwater, OK